RECLAMATION

Managing Water in the West

Hydraulic Laboratory Technical Memorandum
No. YEL-8460-IE-2009-1

Yellowtail Dam Issue Evaluation - Analysis of the Erosion Potential of Flow Overtopping

Pick-Sloan Missouri Basin Project, Montana
Great Plains Region

U.S. Department of the Interior
Bureau of Reclamation
Technical Service Center
Hydraulic Investigations and Laboratory Services Group
Denver, Colorado

September 2009

Mission Statements

The mission of the Department of the Interior is to protect and provide access to our Nation's natural and cultural heritage and honor our trust responsibilities to Indian Tribes and our commitments to island communities.

The mission of the Bureau of Reclamation is to manage, develop, and protect water and related resources in an environmentally and economically sound manner in the interest of the American public.

BUREAU OF RECLAMATION
Technical Service Center, Denver, Colorado
Hydraulic Investigations and Laboratory Services, 86-68460

Technical Memorandum No. YEL-8460-IE-2009-1

Yellowtail Dam Issue Evaluation - Analysis of the Erosion Potential of Flow Overtopping

Pick-Sloan Missouri Basin Project, Montana
Great Plains Region

Prepared: Kathleen H. Frizell
Hydraulic Engineer, Hydraulic Investigations and Laboratory Services, 86-68460

Technical Approval: Robert Einhellig, P.E.
Manager, Hydraulic Investigations and Laboratory Services, 86-68460

Peer Review: Joseph Kubitschek, Ph.D., P.E.
Hydraulic Engineer, Hydraulic Investigations and Laboratory Services, 86-68460

9/23/2009
Date

REVISIONS					
Date	Description	Prepared	Checked	Technical Approval	Peer Review

Contents

Page

Executive Summary

This report describes the analysis of the location and erosive power of the jet impingement on the rock abutments during the potential overtopping of Yellowtail Dam. The analysis used the latest methods (analytical and empirical) available to define jet trajectories and impact zones and estimate the energy available at various impact elevations. This analysis provides information for decision support regarding whether or not the abutments at Yellowtail Dam are adequate to ensure stability of the dam during overtopping events up to 18 feet above the top of the dam parapet walls.

Yellowtail Dam is located on the Bighorn River about 2 miles west (upstream) of Fort Smith, Montana, and about 22 miles north of the Wyoming-Montana state line. Yellowtail Dam, Yellowtail Afterbay Dam, and related structures, constitute the Yellowtail Unit of the Pick-Sloan Missouri Basin Program. Yellowtail Dam was constructed by the Bureau of Reclamation between 1961 and 1966, and impounds Bighorn Lake to provide water for irrigation, flood control, power generation, sediment retention, fishery and waterfowl resource improvement, and municipal-industrial water supply. Bighorn Lake is also a popular destination for fishermen and other recreationists. The dam and power plant are operated by the Bureau of Reclamation.

Yellowtail Dam is a variable-thickness concrete arch structure with an axis radius of 800 ft, a structural height of 525 ft, a hydraulic height of 494 ft, a crest width of 22 ft and a crest length of 1,450 ft at elevation 3660.0. Parapet walls on the dam crest have a top elevation of 3664 ft. Yellowtail Dam controls a drainage basin area of 19,650 mi^2 and the reservoir has a surface area of 12,598 acres with a storage capacity of 1,070,029 acre-feet at the top of joint use elevation 3640 ft. The storage capacity at the top of exclusive flood control elevation 3657 is 1,328,360 acre-feet.

Yellowtail Dam flood routings [16] are summarized in this document and were used in the present analysis of the overtopping events. Overtopping heads of 2, 4, 8, 12, and 18 ft of above the parapet were investigated as requested. The flows were computed for those events using the parameters from the flood routing document.

The 18-ft overtopping event was selected as the maximum event of interest from a risk standpoint. The overtopping flow conditions for the 18 ft of overtopping reservoir head are maximum reservoir 3682 ft, unit discharge 200 $ft^3/s/ft$, brink depth of 7.71 ft over the dam parapet at El. 3664 ft.

The jet characteristics were computed using the 18-ft overtopping event using equations developed for both circular and rectangular jets. A comparison was made of the results. The rectangular jet most closely represents an overtopping jet and the results seemed acceptable; therefore, the rectangular jet equations were used in the remaining analysis.

The results of the jet trajectory analysis for the 18-ft overtopping event are summarized in table A1 of the appendix with the section of the trajectory shown in figure 8, with all the trajectories investigated. The footprints of the locations of the impingement of the jets for the flow rates investigated are shown in figures 9 and 10. The jets from 2 and 4-ft overtopping impinge on the dam, the mid-range overtopping heads impinge high on the abutments, and the 18-ft overtopping head impinge fully along the contact of the dam foundation. The core of the overtopping jet from the 18-ft overtopping event is predicted to be entirely broken up and falling as droplets below about El. 3532 ft with a jet width of 9.7 ft. The jet width was assumed to remain constant with further fall and was used to determine the stream power density below that elevation. Equations for computing mean and fluctuating pressures on the rock surfaces are presented for use if further investigation is requested.

The stream power density, or the erosive power of the water jet, is computed based upon the assumptions regarding the jet characteristics. The stream power density is a function of the area of the jet that impinges on the various surfaces at the various locations. The elevations for the break up of the jet and the associated stream power density are provided for the investigated overtopping heads in table 8. The jets impinge on the dam for small overtopping heads. For mid-range overtopping heads the jets impinge high up on the abutments and onto the power plant. The maximum overtopping head investigated, 18 ft, impinged onto the abutments and onto the power plant at the toe of the dam. Figure 12 shows the plot of the stream power for all the flow rates investigated over the full range of possible erodibility indices for use in the upcoming June 2009 risk assessment. At that time, the team will use judgment about the quality of the rock with the hydraulic characteristics to determine if actual erodibility indices should be developed for Yellowtail Dam rock abutments and the erosive stream power developed from this study applied or if further study is needed.

The following conclusions were drawn from analysis of the range of overtopping heads and flows investigated:

- The analysis of the jet characteristics was conducted with both circular and rectangular jet methodologies because previous overtopping analyses had been performed with circular jet equations converted to rectangular area. It was concluded that an overtopping jet is more similar to a rectangular shape than circular, thus newly published experimentally based rectangular jet equations were used in this analysis [6].
- The overtopping jet for small 2 and 4 ft overtopping heads will impinge on the face of the dam. The trajectories for 8 and 12-ft overtopping will impinge up high on the abutments and on the power plant below. The 18-ft overtopping will impinge upon the rock abutments along the junction with the foundation of the dam and onto the power plant at the toe of the dam. Figures 9 and 10 show the impingement locations. With this locations determined, the type and jointing of the rock exposed to the overtopping jet and flow may be determined in the risk assessment.

- The jet will initially contract, spread, and break up, leading to dissipation of the jet core. Table 5 shows that all the jets will break up at some elevation.
- Engineering judgment is still required to interpret the results of the presented analyzes due to uncertainties associated with the jet characteristics and the accompanying assumptions made. Conclusions were drawn from figure 13 during the risk assessment and are documented in TM No. YEL-8013-RA-2009-1.

Consideration should be given to the fact that there is still quite a bit of uncertainty in the analysis of the jet characteristics and the application of the erodibility index method. The uncertainty has not been quantified in this report, but several short-comings with use of empirically based equations are briefly discussed. Most of the research results to date have been based upon model results, some of which had significant scale effects. How to apply the stream power density computation after jet break up is not known. Judgment was used by maintaining a constant stream power density after jet break up occurred. It would actually be more conservative to assume the continued fall of an intact, continuously widening jet core.

The rock erodibility is based upon estimates of the rock quality using a process developed by Annandale [10]. This method emphasizes the Rock Quality Designation (RQD) and mass strength factors more than joint orientation and shear strength more common to rock abutments. Additional, specific geologic information may not be available for the abutments at Yellowtail Dam, so only estimates based upon judgment might be available if development of erodibility indices is necessary during the risk assessment.

The following recommendations are made as a result of this investigation into the hydraulic loadings from the investigated overtopping events for Yellowtail Dam:

- Further research is recommended on the hydrodynamic characteristics of rectangular free-falling jets, application to the stream power method, and rock characterization using the erodibility index method. Performing this research would significantly reduce the amount of judgment required in the current application of theses methods.

Introduction

These investigations were requested by Robert McGovern, Civil Engineer, Waterways and Concrete Dams Group, 86-68130, to assist with the Issue Evaluation [1], address outstanding SOD recommendations, and assist with the risk assessment of the overtopping failure mode for Yellowtail Dam. This report deals particularly with two SOD recommendations:

- 2005-SOD-A - Complete a comprehensive foundation instrumentation, testing and analysis program to understand the material properties of the breccia zone on the left abutment as well as the discontinuities it contains and how it may affect the stability of Yellowtail Dam for static, hydrologic (including overtopping), and seismic loading conditions.
- 2005-SOD-B - Analyze the results of the Phase II Issue Evaluation studies performed on the foundation and structures at Yellowtail Dam and assess the static, hydrologic, and seismic risk associated with the potential failure modes identified in these studies.

This report documents the analyses performed to date to address the potential failure mode identified as abutment erosion due to overtopping from a range of flood events. The overtopping analysis includes determining the trajectories and impact zones of the requested overtopping heads and flow volumes. The hydraulic loading from overtopping includes determining the jet characteristics during the fall due to gravity, aeration, core break up, and spread.

The hydraulic forces are determined for free-falling jets based upon methodology developed by Ervine, et al [2, 3], Bolaert [4], Wahl [5], and Castillo [6] and utilized previously by Frizell [7, 8, 9]. Annandale's method [10] of determining stream power density is used with the hydraulic loading expected as the jet falls and impinges on the rock at various elevations.

Geology plays an important role in determining the erodibility indices and the possibility of material piping through the foundation for the determination of abutment erosion and stability. Jet erosion tests were performed by Wahl **(**9**)** to assist with determining the erodibility of the breccia material and potential for piping of foundation material. Detailed geology for Yellowtail Dam is contained in the final Geology construction Geology report [12], and the Great Plains Regional Geology investigations [13]. Current geologic investigations are reported in TM No. YT- 86-68320-2009-04 [14], and geotechnical investigations reported in TM No. YT-86-68312-2009-1 [15].

However, the erodibility indices for the areas of impingement on the dam abutments had not been developed at the time of the initial writing of this document. The potential for dam overtopping to cause dam failure due to erosion of the abutments was further evaluated in the June 2009 risk assessment using the initial information on stream power

and location of overtopping developed. A summary was added to the end of this report with reference to the risk assessment documentation.

Tailwater studies were not performed for this project and were not necessary for the overtopping investigations because the jet impingement occurs on the dam or rock and not in the pool below the dam.

The body of the report will discuss the methodology used in the hydraulic analyses and provide a summary of the results. The appendix provides detailed tabular results.

Purpose

The purpose of this report is to document the results of the analytical hydraulic investigations regarding overtopping of the dam, including impingement locations of the jet, and the subsequent hydraulic loading on the rock abutments for Yellowtail Dam, Montana. The jet trajectories and jet characteristics including spread and core break up are determined for free-falling jets. The energy available from the unit discharge passing over the dam with the thickness of the jet is then used to develop stream power density at the various elevations of jet impingement. The stream power density is a measure of the erosive power of the water and is related to the rock quality using an erodibility index that will provide guidance on whether or not the rock will erode.

Project Description

Yellowtail Dam

Yellowtail Dam is located on the Bighorn River about 2 miles west (upstream) of Fort Smith, Montana, and about 22 miles north of the Wyoming-Montana state line. Yellowtail Dam, Yellowtail Afterbay Dam, and related structures, constitute the Yellowtail Unit of the Pick-Sloan Missouri Basin Program. Yellowtail Dam was constructed by the Bureau of Reclamation between 1961 and 1966, and impounds Bighorn Lake to provide water for irrigation, flood control, power generation, sediment retention, fishery and waterfowl resource improvement, and municipal-industrial water supply. Bighorn Lake is also a popular destination for fishermen and other recreationists. The dam and power plant are operated by the Bureau of Reclamation.

Yellowtail Dam is a variable-thickness concrete arch structure with an axis radius of 800 feet, a structural height of 525 ft, a hydraulic height of 494 ft, a crest width of 22 ft and a crest length of 1,450 ft at elevation 3660 ft. Parapet walls on the dam crest have a top elevation of 3664 ft. Yellowtail Dam controls a drainage basin area of 19,650 mi^2 and the reservoir has a surface area of 12,598 acres with a storage capacity of 1,070,029 acre-feet

at the top of joint use elevation 3640 ft. The storage capacity at the top of exclusive flood control elevation 3657 ft is 1,328,360 acre-feet. Figures 1 and 2 show a plan view of the dam with the hydraulic structures and a close up section of the top of dam, respectively.

The spillway is located in the left abutment about 800 feet upstream from the left end of the dam. The spillway consists of an unlined approach channel, a gated intake structure, a concrete-lined tunnel, and a stilling basin with flip bucket. Spillway flows are controlled at the spillway intake structure by two 25-ft-wide by 64.4-ft-tall radial gates, which are separated by a center pier and splitter wall for about 50 feet downstream from the crest. The spillway crest is a concrete ogee section with a crest elevation of 3593 ft.

The spillway tunnel is at an angle of 55º to the horizontal and transitions from square at the entrance portal to a 40.5-ft diameter circular section 105 ft downstream from the portal, then transitions to 32 ft in diameter 145 ft further downstream, and continues for another 1,477.5 ft to the exit portal at the stilling basin. The spillway stilling basin structure is about 205 ft long and 32 ft wide, with a 32-ft-diameter semicircular bottom. The minimum invert elevation of the stilling basin is 3145 ft, and the top elevation of the stilling basin walls is 3204 ft. A hoist, trolley, frame and stoplog slots are located at the downstream end of the stilling basin to provide the capability to dewater the stilling basin for inspection and repairs.

The spillway discharge capacity is 92,000 ft^3/s at reservoir water surface elevation 3660 ft. At spillway discharges up to 12,000 ft^3/s, energy is dissipated by the hydraulic jump contained within the stilling basin; at discharges exceeding 12,000 ft^3/s, the hydraulic jump is swept out of the stilling basin, and the stilling basin acts as a flip-bucket energy dissipater.

The maximum historic reservoir water surface elevation of 3656.3 ft occurred on July 6, 1967. The maximum historic releases from the reservoir of 24,721 ft^3/s (combined spillway and power plant) occurred on July 8, 1967. After this large snow-melt flood caused cavitation damage to the spillway, an aeration slot was constructed into the inclined portion of the tunnel at spillway Station 7+79. In order to maintain free flow conditions in the tunnel and prevent the air slot from becoming submerged which could lead to cavitation damaging the concrete lining, there is currently a requirement that the spillway gates are to have symmetrical operation with a minimum gate opening of 6-in.

The outlet works is located within block 17 of the dam near the right abutment. Two outlet pipes are provided, one on top of the other. The upper outlet is an 84-in-diameter steel pipe with an intake at centerline elevation 3400 ft that is used for making irrigation releases when the power plant is not operating. The lower outlet is also an 84-in-diameter steel pipe with an intake at centerline elevation 3300 ft that is used for reservoir evacuation releases. Discharge capacities of the upper (irrigation) and lower (evacuation) outlets with the reservoir at the top of joint use elevation 3640 ft, are 3,970 ft^3/s and 4,090 ft^3/s, respectively. The combined discharge capacity of these outlets is approximately 5,000 ft^3/s at reservoir water surface elevation 3547 ft. The releases from both outlets are controlled by 84-inch hollow-jet valves located within the power plant structure that

discharge into a stilling basin. The entrances to the outlets are protected by a semicircular reinforced concrete trashrack structure provided with structural steel trashracks. A bulkhead gate on the upstream face of the dam allows for closure of either outlet. The outlet works is rarely used since the operation of the outlet valves causes nitrogen super-saturation in the Bighorn River, harming the downstream fish population. The spillway is now the primary means of making releases beyond the capacity of the power plant units.

The other primary features of Yellowtail Dam include the penstocks and power plant. The power plant is located immediately downstream from the dam at the center of the river. Each penstock has a trash-racked vertical intake structure on the upstream dam face and the centerline elevation of each penstock at its inlet is 3450.0 feet. A 9.93-foot-wide by 18.98-foot-high fixed-wheel guard gate is mounted on the upstream dam face at each penstock intake. The power plant contains four turbines and generators having a total installed generating capacity of 250 megawatts. Four 12-foot-diameter steel penstocks, one each in dam blocks 13, 14, 15, and 16, supply water to four 62.5 MW turbine-driven generators. The discharge capacity of each unit is approximately 2,000 ft^3/s at the top of joint-use storage at reservoir surface elevation 3640 ft.

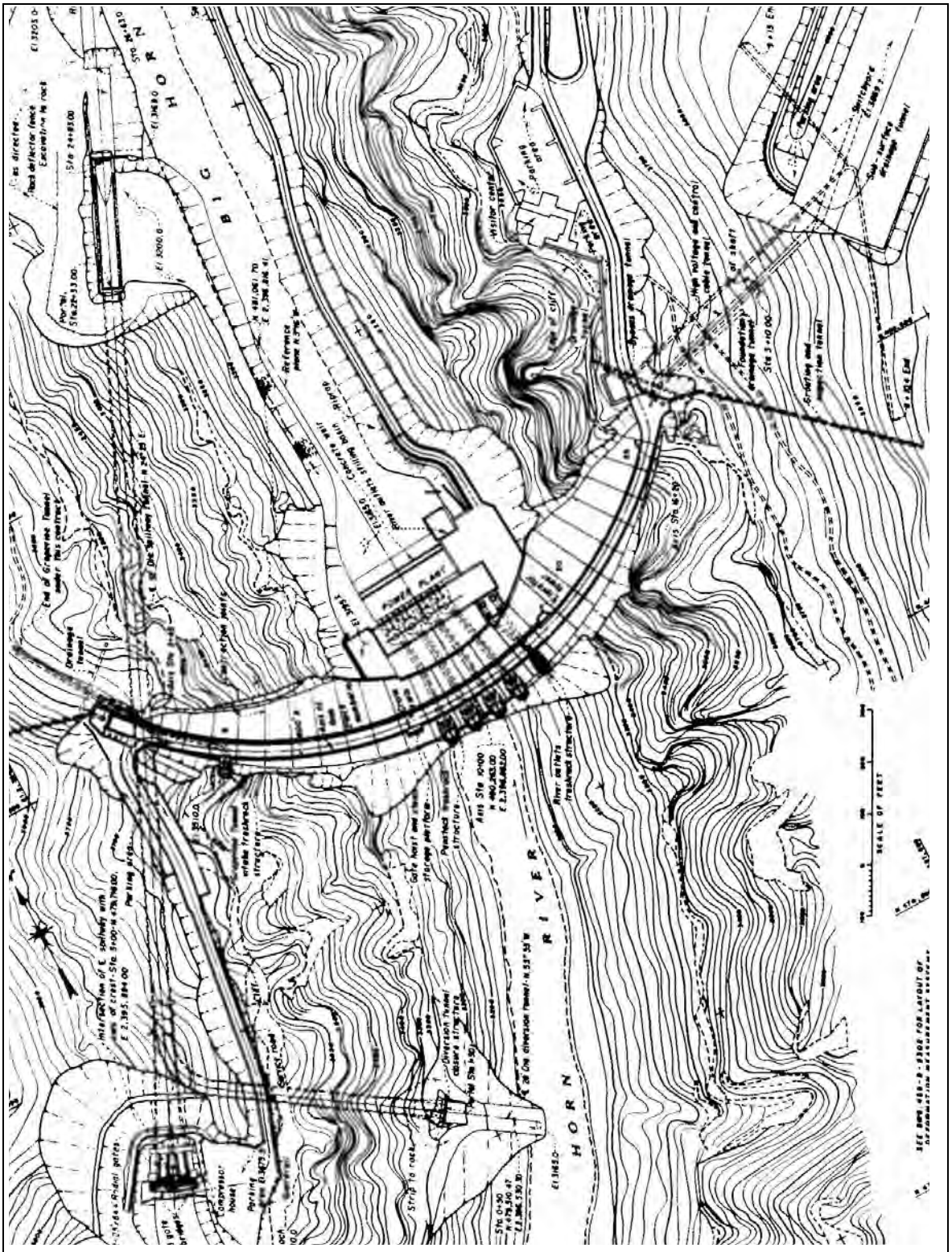

Figure 1. - General plan of Yellowtail Dam showing the spillway tunnel on the left abutment, power plant at the toe of the dam in the center of the river channel, and visitor center downstream from the right abutment.

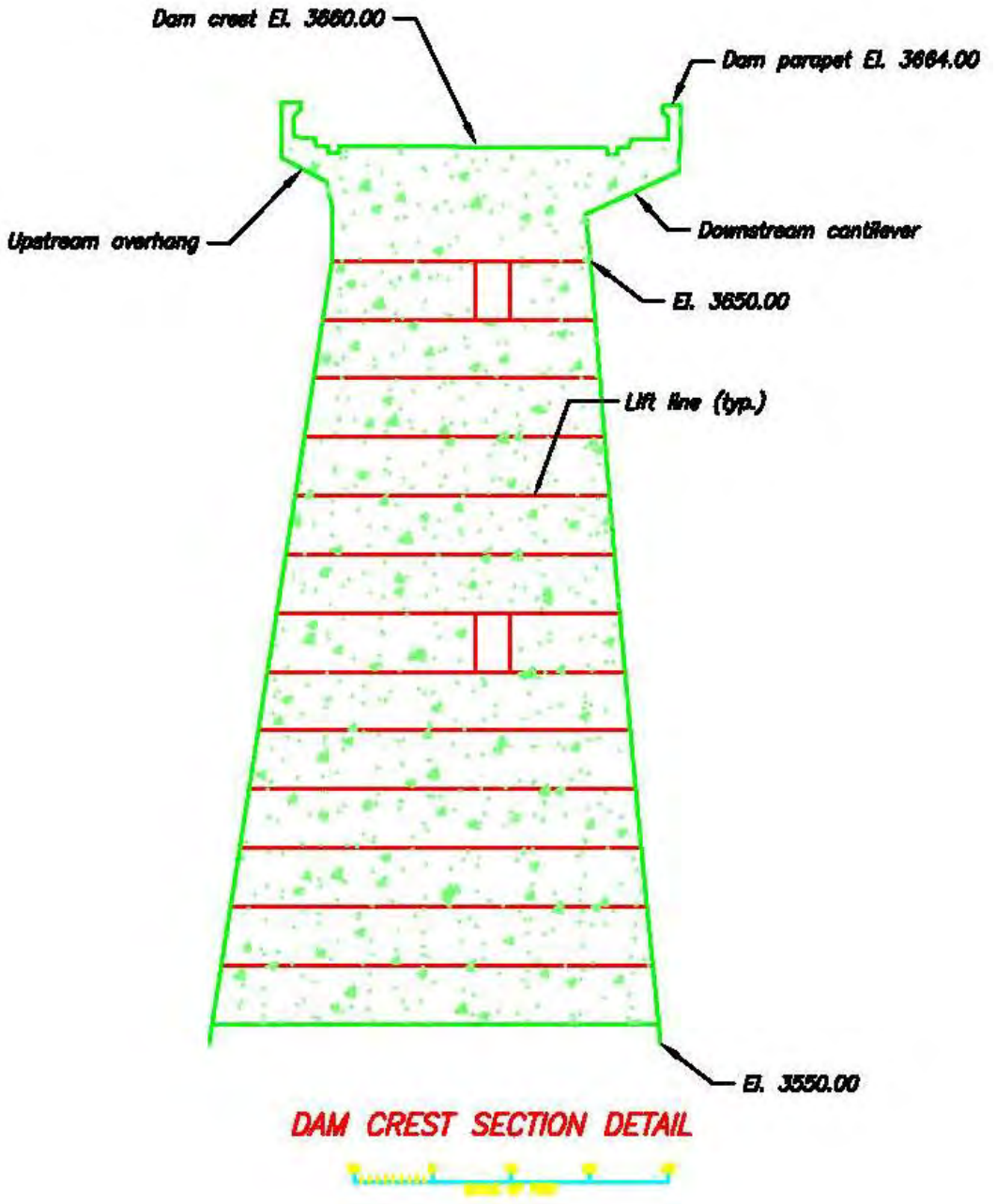

Figure 2. - Enlargement of top of Yellowtail Dam showing the road at El. 3660 ft and upstream and downstream parapet walls at El. 3664 ft. It was assumed that the parapet walls would structurally survive overtopping and that the flow would spring free from the downstream parapet wall.

Geology

The geology description at the site of Yellowtail Dam was obtained from the CFR [1], the Final Construction Engineering Geology Report [12], and the Phase I Issue Evaluation Geology for Foundation Stability and Block Evaluation [13].

Regional Geology

The Bighorn River flows north in a 27-mile-long Bighorn Canyon and joins the Yellowstone River 60 miles to the northeast. The Bighorn Canyon parallels the east side of the Pryor Mountains and has down cut through the dipping sedimentary strata at the northwest end of the Bighorn uplift. The dam is located approximately one mile upstream of the mouth of the canyon. The canyon ends at the margin of the uplifted strata and into a broad river valley. The community of Fort Smith, Montana is located just downstream of the mouth of the canyon.

At the mouth of the Bighorn Canyon uplifted sedimentary strata dip steeply to the northeast. Upstream of the mouth, the strata arch over and have a gentle dip of a few degrees to the northwest at the dam site. Uplift and arching of the strata during the Tertiary Laramide Orogeny caused significant strike slip displacements along high angle discontinuities with deeply grooved slickensides, described as strike-slip shears [13].

Yellowtail Dam is founded entirely on sedimentary strata of the Madison Limestone Formation (Madison Limestone). Early in the investigations, the Madison Limestone was subdivided into three members or units by Reclamation geologists; Upper, Middle and Lower Madison based on local lithologic and slope forming properties.

Site Geology

Yellowtail Dam was founded on bedrock entirely within the Madison Limestone Formation. Unconsolidated alluvial or colluvial deposits overlying bedrock were excavated from the footprint of the dam foundation and a trench excavated into bedrock.

The Madison Limestone is Pennsylvanian age sedimentary limestone and dolomtic limestone and dolomite approximately 1000 ft thick [13]. The Madison Limestone is overlain by the Amsden Formation, which is Missippian age deposit of shale, siltstone and sandstone. The contact of the two formations is marked by an erosional unconformity that is subparallel to bedding, but is a highly irregular surface. The Amsden Formation occurs above the elevation of the dam, but has been a continuing concern because of a large landslide which occurred in the Amsden above the right abutment during construction of the dam.

During sub-aerial exposure during the late Pennsylvanian, extensive dissolution of the Madison created sinkholes, large caves and karst groundwater conduits. Subsequent,

cave collapse breccia and solution breccia filled or partially filled some of the cavities. These breccia deposits are found predominantly in the upper portion of the Madison. Other portions of these karst openings in the upper Madison were subsequently filled with deposits of the Amsden Formation. A second period of dissolution is believed to have occurred at a much later period in geologic time, creating cavities and karst network of openings that are void of deposits and lined with calcite crystals in the middle and lower Madison Limestone.

The upper 500 feet of the Madison have been exposed by erosion of the Bighorn Canyon. The portion exposed at the site was subdivided into 3 members during the early investigations at the dam site. In addition, the Upper member contains extensive deposits of "solution breccia." The characteristics of the 3 members and solution breccia are summarized from two references as follows:

Lower Member – "Rock in this member is chiefly thin to thick bedded, dark gray crystalline limestone with zones being variably dolomitic. Quality of this rock was generally excellent…" [12].

Middle Member – "Topographically this member is characterized by steep inclines, ridges and pinnacled forms. It consists of approximately 200 feet of light gray to buff variably dolomitic limestone. Quality in general is excellent but the topographic features indicate that this member is slightly less resistant to erosion than the lower member" [12].

Upper Member – "…is unconformably overlain by the Amsden Formation, is about 160 feet thick at the damsite. Rock consists of limestone with varied amounts of solution breccia and siltstone stringers" [12]. "It consists of a hard, thick-bedded, pearl-gray to white limestone" [13].

Solution Breccia (within the Upper Madison) – Throughout the upper 80-100 feet of the Madison Limestone and especially noticeable at the base of this zone appears "solution breccia" or material filling what may be collapsed solution cavities. These angular pebbles and cobbles of limestone from the upper Madison Limestone Formation are firmly embedded in a matrix of residual red Amsden Formation "mudstone"[13].

The breccia is described as "chiefly of excellent quality with a few pockets of very good quality solution breccia."

Further information on the dam foundation materials and stability analyses are also available in Technical Memorandums Yellowtail Dam Issue Evaluations No. YT-86-68320-2009-04, Phase 2 – Upper Left Abutment Geology for Foundation Stability Analysis and Karst Breccia Evaluation [14], and No. YT-86-68312-2009-1, Static and Dynamic Foundation Analyses [15].

These geologic investigations were utilized during the June 2009 risk assessment to estimate erodibility indices for the abutments at Yellowtail Dam. A summary of the information was then added to the end of this report.

Flood Routings

Technical Memorandum YEL-8130-IE-2009-1 summarizes flood routings performed for the frequency floods for Yellowtail Dam [16]. The frequency flood hydrographs were developed by the Flood Hydrology Group of the Technical Service Center (TSC) Denver Office in May 2007 [17] and contained values for 100-year up to 10,000,000-year recurrence intervals. The most recent Probable Maximum Floods were developed in 1988 [18] and are considered current. New routings were performed in the current TM and the information used to determine the overtopping discharges for the requested reservoir heads being studied here.

Dam Overtopping Discharges

Discharges through the structures were determined in the same manner as the previous PMF routings which is in accordance with the Standard Operating Procedures (SOP) and the Designer's Operating Criteria (DOC). For Yellowtail Dam, features available for discharge outflow are the dam crest over the parapet wall, the left abutment roadway, the power plant, the outlet works, and the spillway.

Discharges over the parapet wall and left abutment roadway were calculated within the flood routing program using the weir equation, $Q=CLH^{3/2}$ where Q is the discharge in ft^3/s, C is the coefficient of discharge, and H is the head on the crest in feet [19]. A coefficient, C, equal to 2.63 was used in the routings, assuming the dam, parapet wall, or left abutment area acts like a broad-crested weir. The dam crest is at El. 3660 ft with a crest length of 1,450 ft. The parapet wall is at El. 3664 ft and has an approximate crest length of 1,405 ft as measured on the specification drawings. The left abutment roadway is at the same elevation as the dam crest, El. 3660 ft, and has a length of 27 ft. Routings with discharge over the parapet wall assumed the parapet wall would not fail during overtopping, however no specific structural stability studies were performed for the parapet wall. Table 1 shows the results of the flood routings [16].

Table 1. - Summarized flood routing results for Yellowtail Dam overtopping performed for various initial reservoir water surfaces [16].

Reservoir El. (ft)	Overtopping Discharge (ft3/s)	Total Discharge through Dam (ft3/s)	Overtopping Reservoir Head (ft)
Initial Reservoir Water Surface El. = 3614 ft			
3667	18,396	128,309	2.92
3670	54,560	168,831	6.02
3680	246,741	376,020	16.46
3690	478,313	621,039	25.59
Initial Reservoir Water Surface El. =3620 ft			
3667	24,062	134,772	3.49
3671	61,426	176,396	6.51
3681	255,309	385,141	16.84
3690	486,487	629,645	25.88

Reservoir El. (ft)	Overtopping Discharge (ft3/s)	Total Discharge through Dam (ft3/s)	Overtopping Reservoir Head (ft)
Initial Reservoir Water Surface El. =3636 ft			
3669	36,877	149,196	4.64
3672	76,661	193,102	7.55
3682	273,055	404,014	17.61
3690	503,771	647,836	26.49

Table 2 shows the result of the overtopping discharges computed using the same equation, crest length, and discharge coefficient as the flood routing, but for the study reservoir heads of interest.

Table 2. - Summary of parapet wall overtopping discharges computed for requested overtopping heads.

Reservoir El. (ft)	Overtopping Discharge (ft^3/s)	Unit Discharge ($ft^3/s/ft$)	Overtopping Reservoir Head (ft)
3666	10,451	7.44	2
3668	29,561	21.04	4
3670	54,307	38.65	6
3672	83612	59.51	8
3676	153,605	109.33	12
3682	282,189	200.85	18

Figure 3 shows the rating curve for the dam overtopping flows, computed in the flood routings and for this study using the parapet wall elevation of 3660 ft as the crest.

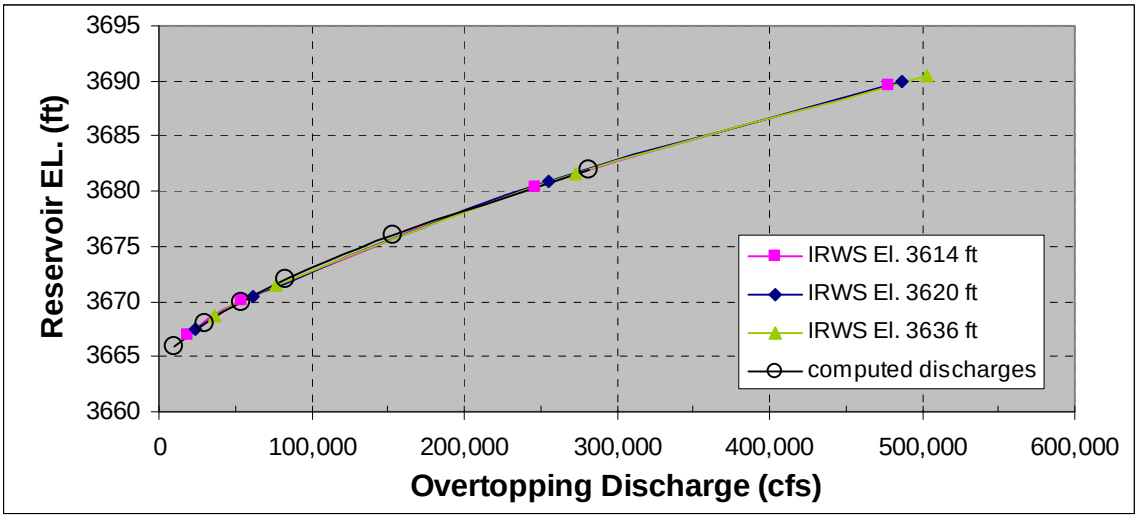

Figure 3. - Discharges overtopping the parapet wall at Yellowtail Dam created during flood routings and computed for the requested reservoir overtopping heads [16].

Hydrodynamic Loading

Reservoir flows over the top of a concrete dam can erode the foundation and the concrete at the toe of the dam and along the abutments. The amount of erosion depends on the duration of flow, the amount of flow, the total height of fall of the overflowing jet of water, the depth of tailwater, and the erodibility of the materials.

The focus of this document is to determine the hydraulic loading associated with overtopping flows under 2, 4, 8, 12, and 18 ft of reservoir head. The flood routings were completed for various frequency events that may or may not have matched these specific overtopping heads [13]. Comparisons of computational methodologies will be made using the 18-ft overtopping event as the worst case. Other overtopping event results will be contained in the body of the report also, with detailed data located in the appendix. The loading is not concerned with the spillway or outlet works flows, but only the amount of water passing over the top of the dam parapet walls. Several aspects of overtopping need to be addressed:

1. The jet characteristics including the jet trajectory, spread, break up of the jet core, and impingement location on the dam, abutments, and power plant at the toe of the dam.
2. Computation of the stream power density associated with each investigated flow rate.
3. Determination of the potential erodibility of the rock abutment material based upon the computed stream power density with flow rate and impingement elevation, and the threshold stream power.

The following are the necessary parameters:

- $Q_{overtop}$ = 282,189 ft^3/s, total duration of overtopping about 3.5 days
- Parapet wall El. 3664 ft
- Top of dam El. 3660 ft
- Elevation at base of dam approximately El. 3135 ft
- Width of dam crest W=22 ft
- Maximum RWS El. 3682 ft with a depth of overtopping above the parapet walls = 18 ft
- Dam crest length L = 1405 ft on an 800-ft radius to the dam axis. Assume the flow will spring free from the parapet wall.
- Tailwater in the river at the toe of the dam (not needed for this project because of impingement locations higher up on the dam and rock).

Definitions

The schematic in figure 4 shows various release situations or possibilities from dams with definition of the important parameters of a free falling jet into a plunge pool or

potentially impacting a surface above the plunge pool shown in figure 5 [4, 5, 6]. The following list includes the parameter definitions for figures 4 and 5:

$B_i = D_i$ = width or diameter of the jet at issuance from the dam
$B_g = D_j$ = jet thickness at impact with the plunge pool or on a surface
$B_j = D_{out}$ = outer dimension of the jet including the inner core of the jet and the jet spread
$d_b = t_i$ = jet thickness or overtopping depth at issuance from the dam
$B_j = t_j$ = jet thickness at impact with the plunge pool or on a surface
$H = H_{overtop}$ = total head above the opening or over the crest
V_i = mean jet velocity at issuance from the dam
V_j = mean jet velocity at impact with the plunge pool or on a surface
Y = total plunge pool depth
Z = difference between upstream and downstream water levels
θ_i = jet angle from horizontal at issuance from the dam
$\delta_{out} = \varepsilon$ = angle of the outer jet spread in a free falling jet
α_{out} = angle of the outer jet spread in the plunge pool

Determination of the jet characteristics is the first step in estimating the erosion or scour potential of the rock based upon the loading caused by the jet at impact with the rock surfaces. Overtopping flows for Yellowtail Dam will be similar to the schematic description given as figure 4a with jet characteristics defined from figure 5 [5, 6].

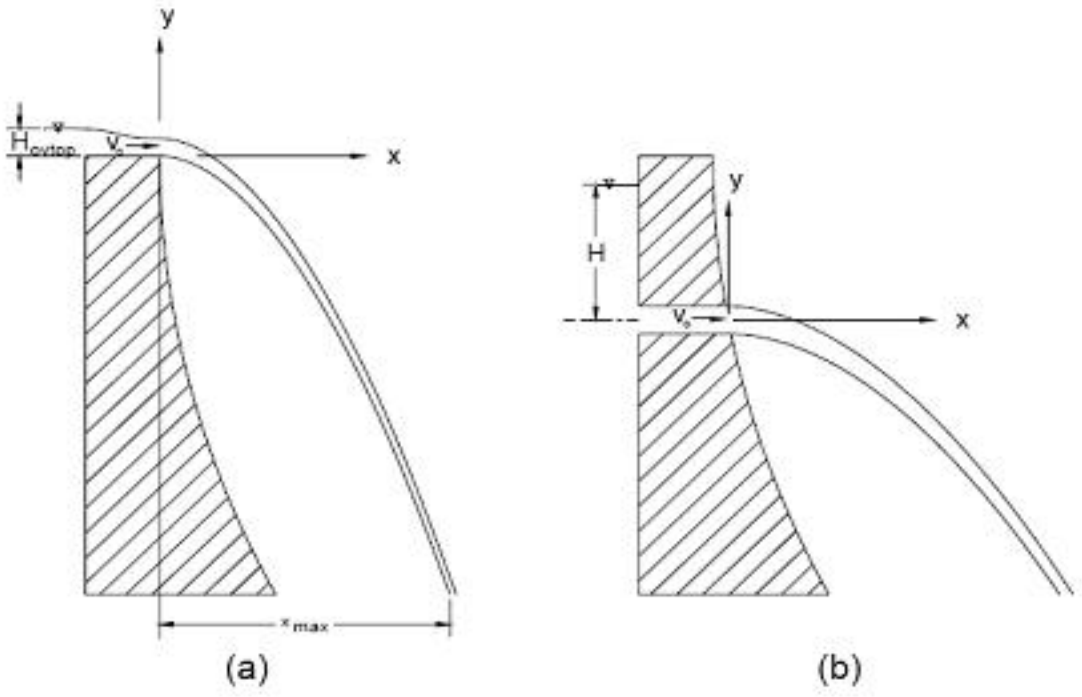

Figure 4 - Potential release scenarios from dams that affect the computation of the characteristics for a free-falling jet through the atmosphere [5].

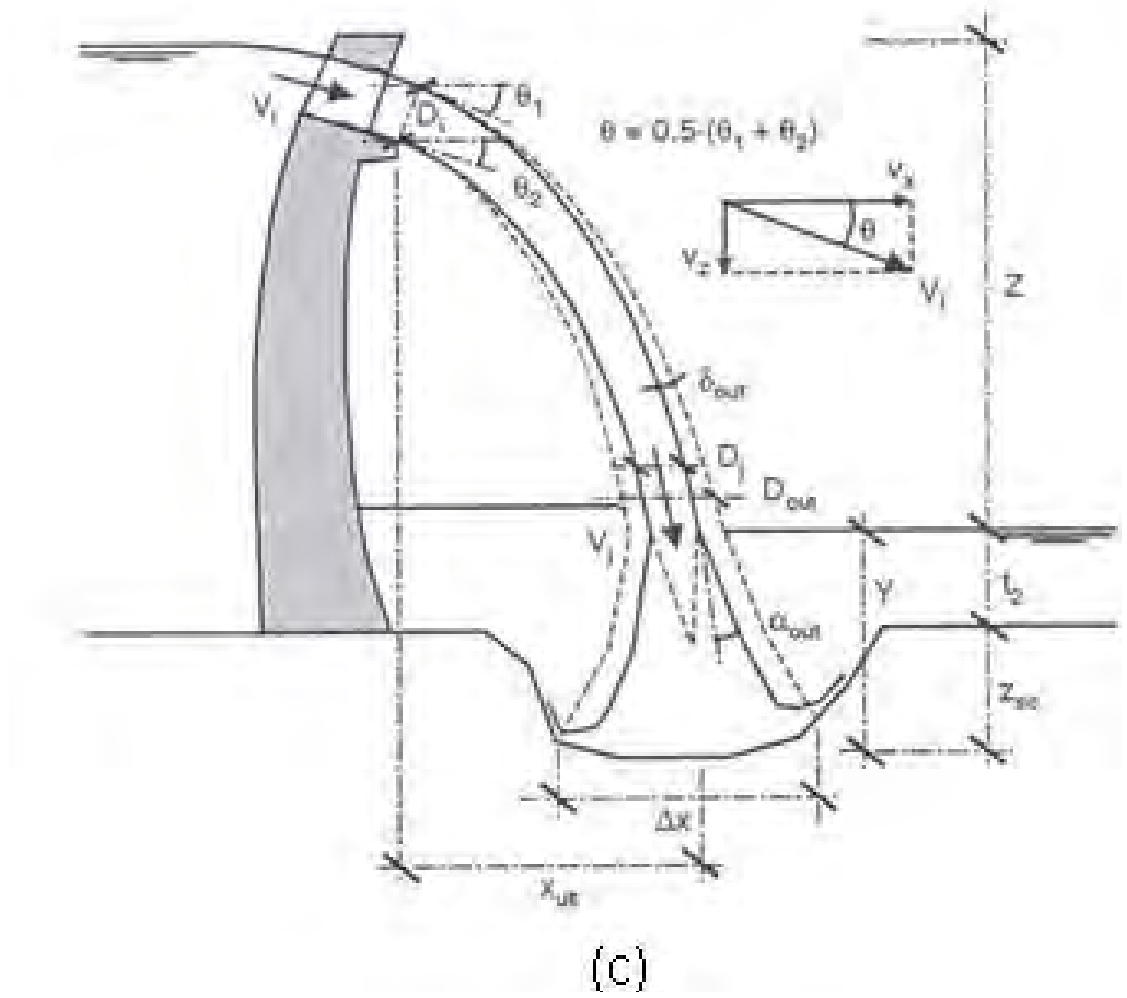

Figure 5. – Definition sketch for parameters of a free falling jet (Bollaert, 2002), (Catillo, 2006).

Trajectory Calculations

The flow over the top of the dam and the free fall of the jet at the various elevations to estimate impingement zones on rock abutments or tailwater plunge points must be characterized. The jet trajectory is computed for the free fall where initial depth and velocity, initial turbulence, and fall length play a role. If there is adequate free fall the jet will begin aerating and spreading. With additional free fall the core of the jet may also begin to break up and dissipate, thus greatly reducing impact on the rock surfaces. Once the free-falling jet enters the tailwater pool, the angle of entry and depth of the tailwater pool affects the jet spread and diffusion. The following sections address the procedures used to determine the jet characteristics.

For Yellowtail Dam overtopping, the initial angle of issuance is zero (i.e. horizontal) and the initial jet thickness or depth of overtopping is the brink depth over the parapet wall

elevation of 3664 ft as the datum. The brink depth and initial velocity are computed using the estimated 18-ft reservoir head event over the dam parapet. The critical flow depth is first computed by the relationship, $d_c = (q^2/g)^{1/3}$, where q is the discharge per unit of crest length [19]. The brink depth is then determined by the relationship developed between the critical and brink depth [20] and continuity. For the 18 ft overtopping of Yellowtail Dam the unit discharge, q = 200.85 $ft^3/s/ft$, the brink depth is equal to the initial depth of overtopping, d_b = 7.71 ft, and the initial mean velocity at the brink is V_i= 26.06 ft/s.

The flow over the top of the dam is simply a free overfall and is computed using the equation of motion for particle trajectory due to gravity, assuming no aerodynamic influences on the jet [4]. Wahl, et al. [5] discusses the use of the brink depth as the initial depth, the brink velocity, and brink velocity head for the computation of the jet trajectory for free overall during an overtopping situation.

The conventional form of the equation of motion produces the following result describing particle trajectory with the downstream edge of the parapet wall as the origin of an x-z coordinate system defining the bottom edge of the jet:

$$z = x\tan\theta_i - \frac{gx^2}{2V_i^2\cos^2\theta_i}$$

This equation is simplified when the jet issues horizontally (e.g. θ_i=0) from the top of the dam to:

$$z = -\frac{gx^2}{2V_i^2}$$

Further manipulation of the equation may be performed by writing it in terms of the velocity head, $h_v = V_i^2/2g$, producing:

$$z = -\frac{x^2}{4h_v}$$

This equation approximates the lower free surface of the jet. The upper or outer edge of the jet is then defined by adding the initial jet thickness, equal to the brink depth, to the bottom edge of the jet.

The above equations of motion do not account for contraction and expansion of the jet prior to plunge into the tailwater pool or impingement on the rock. Nor do they include aerodynamic effects which are likely significant. In the case of Yellowtail Dam with free overflow conditions, the horizontal travel and vertical drop of the jet will determine the location of the impingement. Table 3 shows the result of the trajectory calculations for Yellowtail Dam under 18 ft of reservoir head with the initial jet thickness shown as the

brink depth. Figure 6 is a side view of the range of free-falling jet trajectories with no spread of the outer diameter of the jets shown.

Table 3. - Free fall trajectory locations for the 18 ft overtopping event at Yellowtail Dam with x (horizontal) and z (vertical) distances and elevations from the downstream parapet location and elevation. Vertical fall continues as if unimpeded by abutments or tailwater and does not include any other jet characteristics, such as spread or break up.

Drop z ft	Distance from d/s parapet x ft	El. Lower nappe ft	El. upper nappe ft	Drop z ft	Distance from d/s parapet x ft	El. Lower nappe ft	El. upper nappe ft	Drop z ft	Distance from d/s parapet x ft	El. Lower nappe ft	El. upper nappe ft
0	0.00	3664	3671.71	-145	78.20	3519	3526.71	-355	122.36	3309	3316.71
-1	6.49	3663	3670.71	-150	79.54	3514	3521.71	-360	123.22	3304	3311.71
-2	9.18	3662	3669.71	-155	80.85	3509	3516.71	-365	124.07	3299	3306.71
-3	11.25	3661	3668.71	-160	82.15	3504	3511.71	-370	124.92	3294	3301.71
-4	12.99	3660	3667.71	-165	83.42	3499	3506.71	-375	125.76	3289	3296.71
-5	14.52	3659	3666.71	-170	84.67	3494	3501.71	-380	126.59	3284	3291.71
-6	15.91	3658	3665.71	-175	85.91	3489	3496.71	-385	127.42	3279	3286.71
-7	17.18	3657	3664.71	-180	87.13	3484	3491.71	-390	128.25	3274	3281.71
-8	18.37	3656	3663.71	-185	88.33	3479	3486.71	-395	129.07	3269	3276.71
-9	19.48	3655	3662.71	-190	89.52	3474	3481.71	-400	129.88	3264	3271.71
-10	20.54	3654	3661.71	-195	90.69	3469	3476.71	-405	130.69	3259	3266.71
-14.64	24.85	3649.36	3657.07	-200	91.84	3464	3471.71	-410	131.50	3254	3261.71
-15	25.15	3649	3656.71	-205	92.98	3459	3466.71	-415	132.30	3249	3256.71
-20	29.04	3644	3651.71	-210	94.11	3454	3461.71	-420	133.09	3244	3251.71
-25	32.47	3639	3646.71	-215	95.22	3449	3456.71	-425	133.88	3239	3246.71
-29.27	35.13	3634.73	3642.44	-220	96.32	3444	3451.71	-430	134.67	3234	3241.71
-30	35.57	3634	3641.71	-225	97.41	3439	3446.71	-435	135.45	3229	3236.71
-35	38.42	3629	3636.71	-230	98.49	3434	3441.71	-440	136.22	3224	3231.71
-40	41.07	3624	3631.71	-235	99.55	3429	3436.71	-445	136.99	3219	3226.71
-45	43.56	3619	3626.71	-240	100.61	3424	3431.71	-450	137.76	3214	3221.71
-50	45.92	3614	3621.71	-245	101.65	3419	3426.71	-455	138.52	3209	3216.71
-55	48.16	3609	3616.71	-250	102.68	3414	3421.71	-460	139.28	3204	3211.71
-58.55	49.69	3605.45	3613.16	-255	103.70	3409	3416.71	-465	140.04	3199	3206.71
-60	50.30	3604	3611.71	-260	104.71	3404	3411.71	-470	140.79	3194	3201.71
-65	52.36	3599	3606.71	-265	105.72	3399	3406.71	-475	141.54	3189	3196.71
-70	54.33	3594	3601.71	-270	106.71	3394	3401.71	-480	142.28	3184	3191.71
-75	56.24	3589	3596.71	-275	107.69	3389	3396.71	-485	143.02	3179	3186.71
-80	58.09	3584	3591.71	-280	108.67	3384	3391.71	-490	143.75	3174	3181.71
-85	59.87	3579	3586.71	-285	109.63	3379	3386.71	-495	144.49	3169	3176.71
-87.82	60.86	3576.18	3583.89	-290	110.59	3374	3381.71	-500	145.21	3164	3171.71
-90	61.61	3574	3581.71	-295	111.54	3369	3376.71	-505	145.94	3159	3166.71
-95	63.30	3569	3576.71	-300	112.48	3364	3371.71	-510	146.66	3154	3161.71
-100	64.94	3564	3571.71	-305	113.42	3359	3366.71	-515	147.38	3149	3156.71
-105	66.55	3559	3566.71	-310	114.34	3354	3361.71	-520	148.09	3144	3151.71
-110	68.11	3554	3561.71	-315	115.26	3349	3356.71	-525	148.80	3139	3146.71
-115	69.64	3549	3556.71	-320	116.17	3344	3351.71	-530	149.51	3134	3141.71
-120	71.14	3544	3551.71	-325	117.07	3339	3346.71	-535	150.21	3129	3136.71
-125	72.61	3539	3546.71	-330	117.97	3334	3341.71	-540	150.91	3124	3131.71
-130	74.04	3534	3541.71	-335	118.86	3329	3336.71	-545	151.61	3119	3126.71
-131.73	74.54	3532.27	3539.98	-340	119.75	3324	3331.71	-550	152.30	3114	3121.71
-135	75.46	3529	3536.71	-345	120.62	3319	3326.71				
-140	76.84	3524	3531.71	-350	121.49	3314	3321.71				

Free Jet Spread and Potential for Jet Core Decay

The core of the free-falling jet will experience initial contraction due to gravitational acceleration, then gradually dissipate, and spread as the jet breaks up with adequate fall distance. If the jet were to impact the tailwater other factors would combine to influence the decay of the core and spread or diffusion of the outer edges of the jet, but this will not occur at Yellowtail Dam because of the location of the jet impact.

The fall height of an overtopping jet varies across the width of the dam, depending on whether the jet impinges on the abutments, the dam, or falls to the tailwater. For

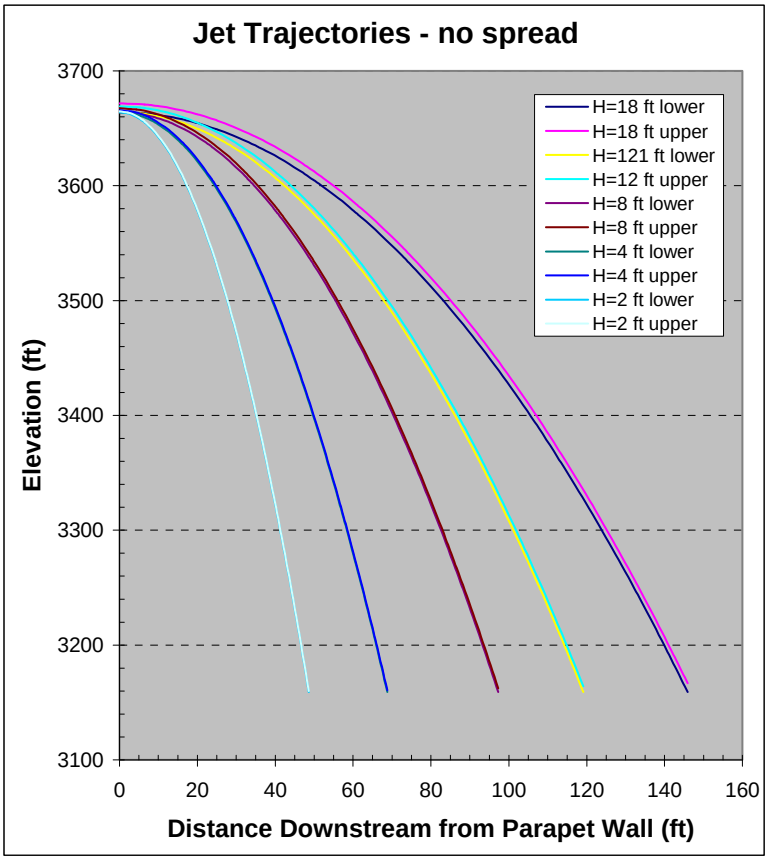

Figure 6. - Sectional view of the trajectory profiles, with equations of motion only, for the overtopping head range investigated for Yellowtail Dam. (Note the trajectories all originate at the downstream parapet wall on the top of the dam road.)

Yellowtail Dam, the fall height under the maximum overtopping event is computed as the difference between maximum reservoir El. 3682 ft and the impingement location whether on the abutments or on the power plant. The impingement on the rock due to the falling jet is computed, but in addition to that is the accumulation or potential concentration of the jet as it flows over the abutments. This is not accounted for in this analysis and could be important in the potential for erosion and will be discussed during the risk assessment.

The jet characteristics change as the jet overtops the dam and falls freely. The flow is initially turbulent and accelerating as it passes over the dam crest. When this flow passes the downstream parapet, the lower boundary separates and the flow becomes a free jet that continues to accelerate and contract due to gravity as it falls. At some point during the free-fall turbulent fluctuations in velocity and interactions at the air-water interface result in the onset of instability producing the rapid growth of free-surface disturbances which are sheared off as droplets giving way to air entrainment. This initial breakup process continues to migrate toward the intact core of the jet as it falls, eventually terminating in a fully disintegrated jet or spay comprised of a range of droplet sizes. The

droplets continue to interact in a process of continued coalescence and breakup and the fully aerated jet continues to spread. If the free-fall height is sufficiently large, the spray is expected to reach terminal velocity due to aerodynamic drag imparted to the diverging droplets. The entire process dissipates energy that would otherwise be available if the jet remained intact.

Much research has been conducted on free-falling circular jets. Equations developed from that research have been primarily used in previous overtopping analyses with adaptations made for the rectangular jet characteristics typical of an overtopping flow [7, 10, 11]. It was assumed that rectangular jets would behave similarly to round jets during a free fall. During this analysis, newly discovered rectangular jet equations [6] were compared with the computations using the circular jet equations [3,4,10]. The 18-foot reservoir overtopping head results are shown in the following sections for comparison.

The state of the jet maybe described by the empirical equations determined to predict jet spread, D_{out} (circular) or B_j,(rectangular), break up, L_b, and the length of the fall, L_j. The core of the jet will not be intact if the break up distance, L_b, is less than the fall distance, L_j, to the location of interest.

Rectangular Jet Computations

In previous studies it was assumed that rectangular jets would behave similarly to round jets during a free fall. However, it is not known if this is a valid or reasonable assumption, nor how well the equations will predict behavior. Therefore, when additional research results and methodology on rectangular jet characteristics became available it was incorporated into this analysis [6]. The previous section on definitions shows the comparison between the parameters for circular and rectangular jets.

The width of a rectangular jet at the point of impingement due to gravitational contraction plus the jet spread, caused by aeration of a turbulent jet, has been presented by Castillo [6] and is given by:

$$B_j = B_g + 2\varepsilon$$

where the equation for B_j is of the same form as D_{out} for circular jets with slightly different parameters defined as follows:

$$B_g = \frac{q}{\sqrt{2gZ}}$$

where B_g is the contraction of the jet during fall due to gravity and

$$\varepsilon = 4\varphi\sqrt{d_b}\left[\sqrt{Z} - \sqrt{d_b}\right]$$

which is the component of jet spread based upon the initial brink depth, the jet turbulence, and the total height of the fall. The parameter φ is a function of the turbulent intensity, T_u^* that includes the unit discharge of the flow and the initial conditions, IC, defined as follows:

$$\varphi = 1.07T_u^* \text{ with } T_u^* = \frac{q^{0.43}}{IC}$$

where q is unit discharge in metric units. The initial conditions at the top of the dam, IC, are defined by several constants:

$$IC = \frac{14.95g^{0.5}}{K^{1.22}C_d^{0.19}}$$

where again in metric units $C_d = 1.7$ and $K = 0.85$.

Combining the parts of these equations provides the following equation for the width of the rectangular free-falling overtopping jets with gravitational and turbulence causing jet spread at Yellowtail Dam:

$$B_j = \frac{q}{\sqrt{2gZ}} + 4\varphi\sqrt{d_b}\left[\sqrt{Z} - \sqrt{d_b}\right]^1$$

[1] *The original work called for h_o which was defined as approximately equal to 2h defined as the energy head. Wahl [5] showed that this definition was not correct for overtopping situations; therefore, d_b was substituted and produced more reasonable results than computations using the energy head.*

For jet core break up, the constant was slightly modified from the circular jet equation [3] for use with a rectangular jet by Castillo [6]. The length to break up of the core of a rectangular jet is given as:

$$L_b = 0.85\frac{B_i F_i^2}{\left(1.07T_u F_i^2\right)^{0.82}}$$

where T_u is the turbulence intensity of the jet based upon values from table 4 for various types of jet issuance. For an overtopping event, the jet thickness and the characteristics led to selection of an initial turbulence intensity, $T_u = 0.03$ from table 4 for a free overfall.

Table 4. - Table of initial turbulence intensities for free falling jets Bollaert (2002). The turbulence intensity is assumed constant through the fall.

Structure type	Turbulence Intensity
free overfall	0.00-0.03
ski jump	0.03-0.05
Valve	0.03-0.08

The length of free fall for break up of the rectangular jet core, L_b, is equal to 132 ft which corresponds to El. 3532 ft for the 18-ft overtopping event. Full jet break up implies that the flow no longer is a coherent mass of water and thus will add little or no additional impact pressure to surfaces below the break up El. 3532 ft upon impingement.

Theoretical Results Comparison

The jet spread and break up characteristics for a free-falling overtopping jet using the rectangular jet equations as defined were computed and are shown on figure 7 with those from the circular jet computations [2, 3, 10] for the 18 ft overtopping event. The forms of

the circular and rectangular equations used to predict jet characteristics are very similar. Both include a gravitational term and the term for jet spread caused by turbulence and aeration during the fall when determining the jet width. The circular jet equations show that the jet spreads less during the fall.

The length to break up of the core of a rectangular jet and circular jet is the same, other than a difference in the constants that provide a longer fall distance for the circular jet till breakup by a factor of 1.18. The length of free fall for break up of the circular jet core for the 18-ft overtopping event would; therefore, equal 155 ft corresponding to El. 3509 ft. Based upon the computations for jet break up, the rectangular overtopping jet would break up sooner than a circular jet.

These results might also be supported by the computation of an equivalent circular diameter from the rectangular area produced by unit width and a given overtopping depth. This would produce a more compact circular core than a thin rectangular jet, thus it would seem that a rectangular jet would spread quicker and break up sooner.

The rectangular jet geometry most closely replicates an overtopping jet and the results from the compared methodologies support use of the rectangular jet equations developed by Castillo [6] were used for determining the jet characteristics for Yellowtail Dam overtopping heads of 2 to 18 ft.

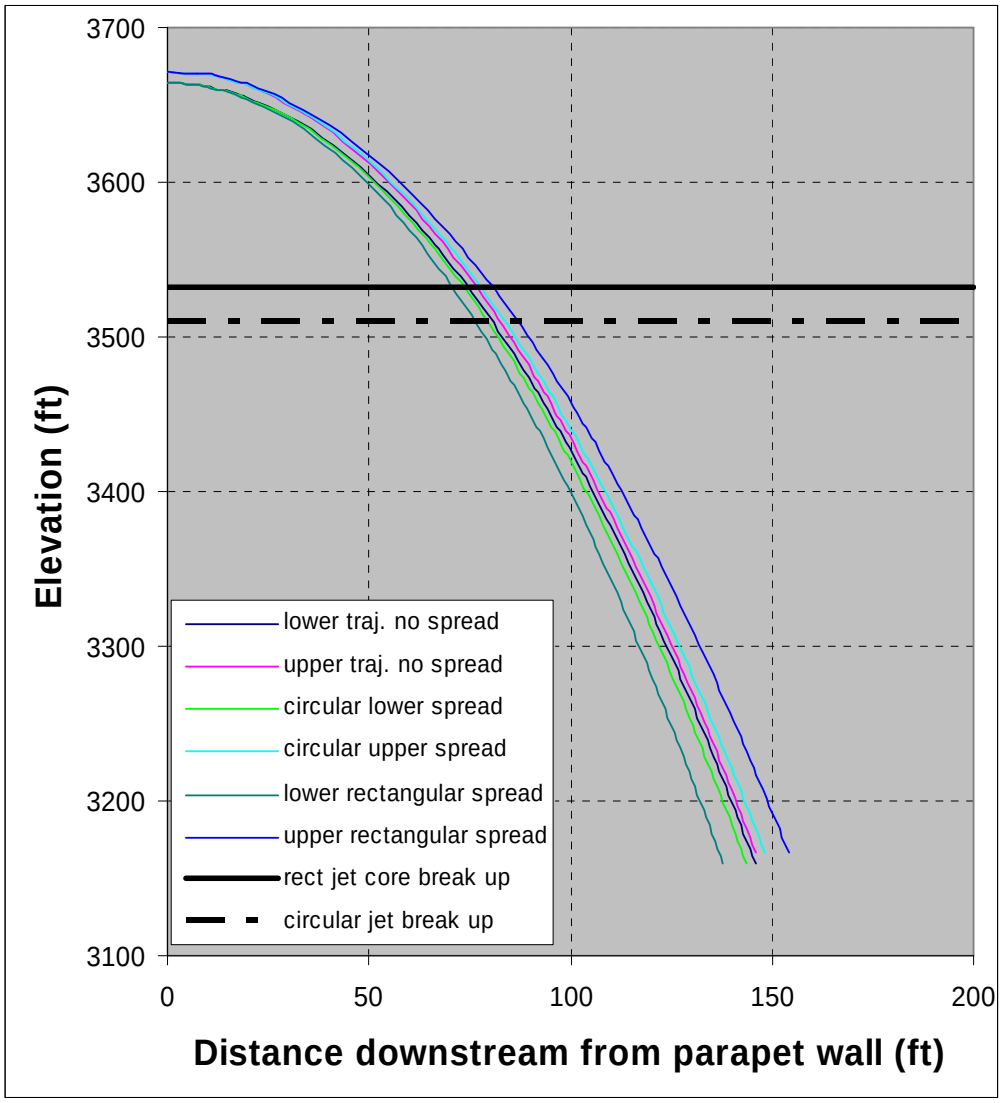

Figure 7. - Comparisons of the jet trajectories for 18 ft of overtopping head computed by equations developed for circular and rectangular jets. Also shown are the elevations of jet break up for the overtopping event using circular and rectangular jet equations.

Jet Trajectories for Overtopping Flows Using Rectangular jet Equations

Results of the rectangular jet trajectory computations for 2 to 18 ft of overtopping with the jet spread and break up predicted are shown on figure 8. Tables A1-A5 provide the details of the jet trajectory locations and widths. Figure 8 may be compared to figure 6 to see the influence of turbulence and spread on the thickness of the jets.

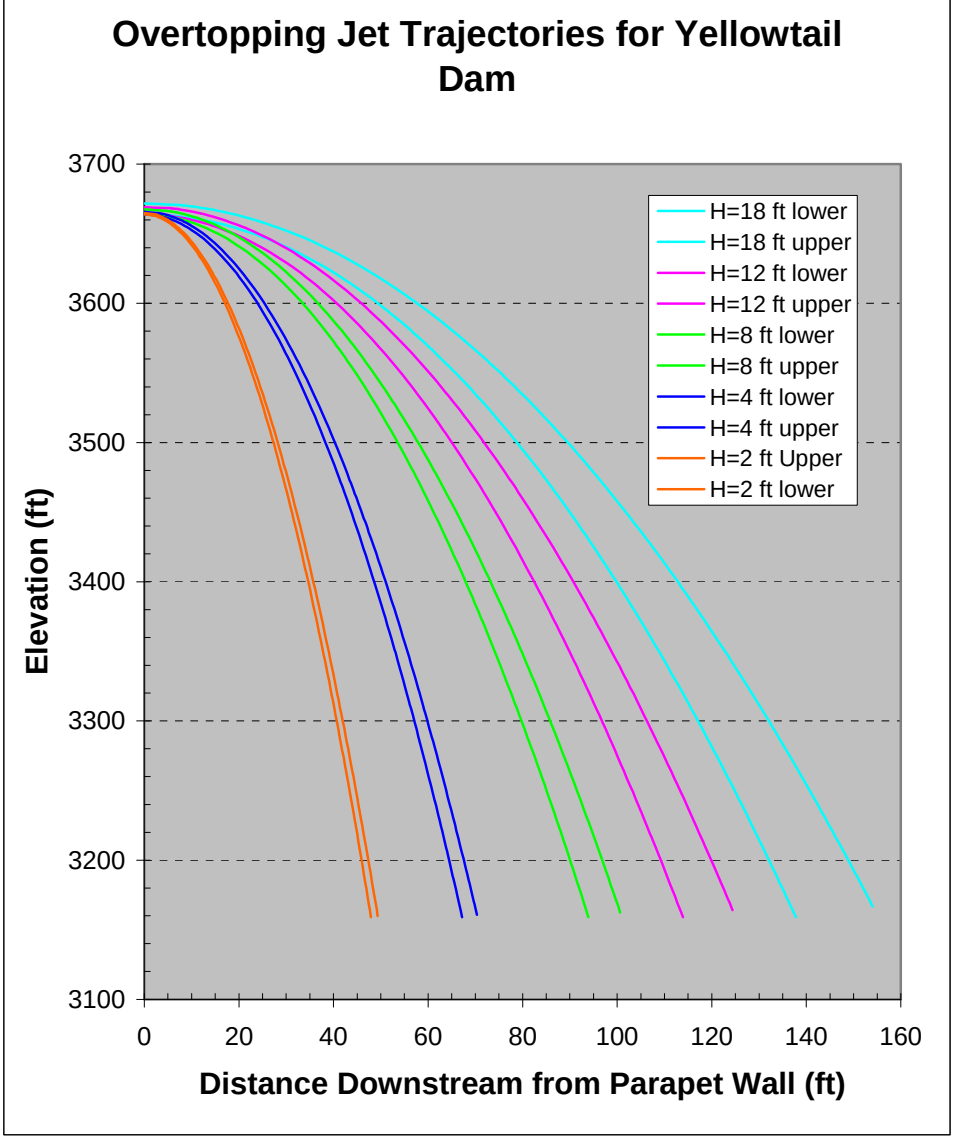

Figure 8. - Jet trajectories for Yellowtail Dam including the projected spread of the jet as it falls through the air using the rectangular jet equations for spread.

Figures 9 and 10 show the predicted footprints of jet impingement, including the spread of the jets, on the downstream face of the dam, the rock abutments, or the power plant. The overtopping jets impinge on the downstream dam face for the smaller overtopping events, and on the rock abutments and power plant for higher overtopping events due to the shape of the arch dam and the overhanging roadway at the top of the dam. The plot was developed by using the radius of the arch dam to offset the trajectory with the computed jet spread using the intersection points with the contours. These plots may be used to visualize the locations of impingement for making judgement about the need to further investigate pressures on important fault zones or rock joints and stream power density on rock materials in the impingement zones.

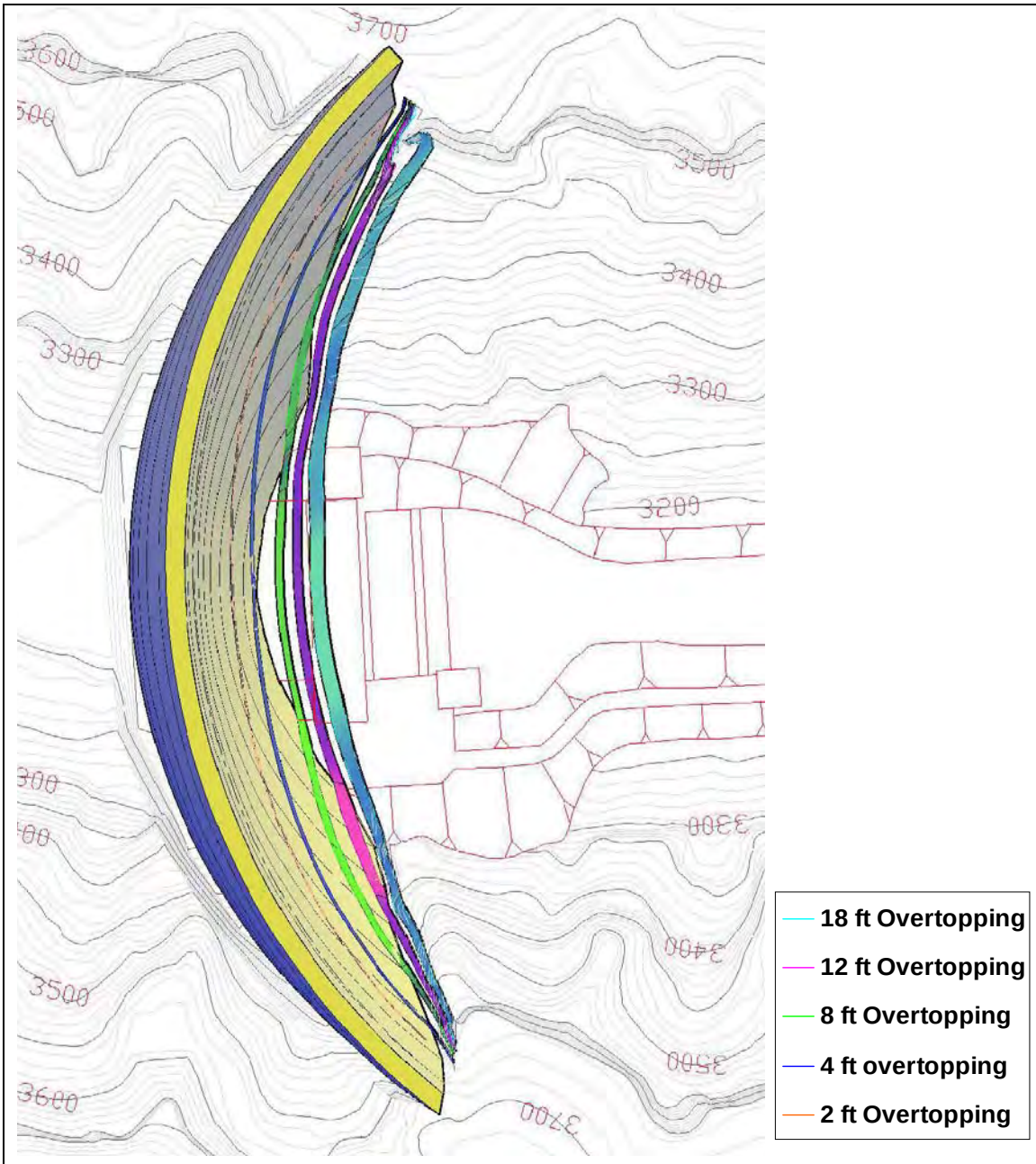

Figure 9. - Plan view of the footprint of the trajectories for Yellowtail Dam projected to catch points with the dam and the topography. The trajectories include the projected spread of the jet as it falls. It appears that the 8, 12, and 18 ft overtopping trajectories impinge, at least high up on the abutments and the power plant at the base of the dam. The trajectories for the 2 and 4 ft of overtopping heads will land on the face of the dam.

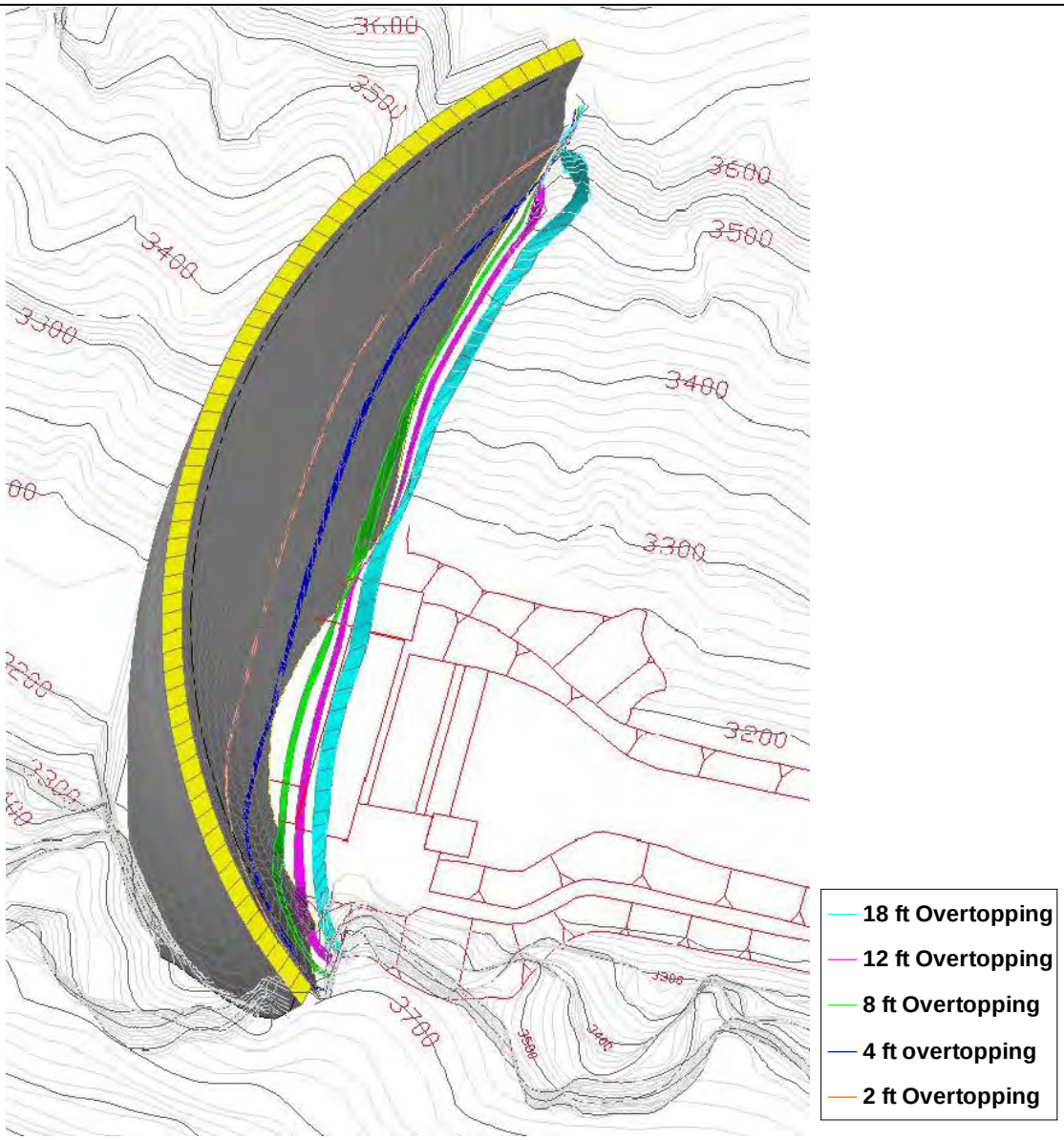

Figure 10. - Isometric view of the trajectories impingement locations for the overtopping events of 2, 4, 8, 12 and 18 ft of head for Yellowtail Dam.

Table 5 shows the rectangular jet core will break up fairly high on the abutments but will still impinge on the rock prior to break up for the higher overtopping heads. The jet break up lengths predicted don't include the possibility of the droplets coalescing following break up of the core. If coalescence were to occur, then potentially the water may impact on the abutment surfaces with slightly more force; however, no research results are available in this field.

Table 5. – Length to break up of the jet core using the rectangular jet equation for the various flow rates being investigated.

Head	q	L_b	
(ft)	(ft^3/s/ft)	(ft)	(EL.ft)
2	7.44	14.64	3649.36
4	21.04	29.27	3634.73
8	59.51	58.55	3605.45
12	109.33	87.82	3576.18
18	200.85	131.73	3535.27

Investigations of the jet trajectories for other flood events were performed for use, if needed; in risk determination of other than erosion under the maximum 18 ft of overtopping discussed here. The trajectories and jet widths for the 2, 4, 8, 12, and 18 foot of overtopping head and discharges from table 2 are shown in appendix A.

Pressure Forces on the Rock

The simplest method to evaluate pressures on a joint in a rock mass is to determine the stagnation pressure at the surface of the rock mass and transfer that to the bottom of the joint. Therefore, the total pressure at the bottom of the joint would be the velocity head plus the depth of the joint. This method assumes no friction or loss as the water travels down the joint and would be conservative for most applications. It could be used to get an initial idea of the potential uplift and whether or not rock masses may become unstable due to uplift. Velocities have been computed at a wide range of elevations and may be used to determine forces on rock joints, if determined necessary during the future risk assessment.

The total dynamic pressure acting on the surface is a function of the empirically derived pressure coefficients and the velocity head [3, 4, 6]:

$$P_{\max} = \left(C_p + C_p^{'}\right)\gamma\phi\frac{V^2}{2g}$$

The mean dynamic pressure coefficient, C_p, is given by:

$$C_p = ae^{-b\left(Y/\ B_j\right)}\ for\ Z/L_b > 0.5$$

$$C_p = 0.36\left(Z/L_b\right)^{-1.04}\ for\ Z/L_b < 0.5$$

where Z equal to the head differential from the reservoir to the surface or pool. Table 6 is the table of empirically derived constants for the above equations.

Table 6. – Constants based upon fall height, jet length to break up, and plunge pool depth for the mean dynamic pressure coefficient. C_p is constant for a given ratio of Z/L_b if no plunge pool.

Z/L_b	a	b	Cp for $Y/B_j \leq 4$
<0.5	0.98	0.07	0.78

Z/L_b	a	b	Cp for $Y/B_j \leq 4$
0.5-0.6	0.92	0.079	0.69
0.6-0.8	0.65	0.067	0.5
1.0-1.3	0.65	0.174	0.32
1.5-1.9	0.55	0.225	0.22
2.0-2.3	0.5	0.25	0.18
>2.3	0.5	0.4	0.1

The fluctuating dynamic pressure coefficient, $C_p^{'}$, for impact on a surface or plunge pool with shallow depth compared to the jet width [3, 4, 6] and table 7 with constants is given by:

$$C_p^{'} = a(\frac{Y}{B_j})^3 + b(\frac{Y}{B_j})^2 + c(\frac{Y}{B_j}) + d \quad \text{for } Y/B_j<14$$

Table 7. - Constants based upon fall height, jet length to break up, and plunge pool depth for the mean dynamic pressure coefficient.

Z/L_b & $Y/B_j<14$	A	b	c	d	Type of jet
<1.4	0.0003	-0.0104	0.09	0.083	Compact-developed - disintegrated
1.5 – 2	0.0003	-0.0094	0.0745	0.05	Developed-disintegrated
>2	0.0002	-0.0061	0.0475	0.01	Developed-disintegrated

Because there is no jet plunging into a pool at the toe of Yellowtail Dam only the potential for impact on the rock surfaces might be needed.

In addition, these pressure coefficients may vary depending upon the characteristics of the crack geometry. For open-ended cracks the uplift is characterized by multiplying the stagnation pressure by a coefficient that is a function of the tailwater pool depth and jet thickness. For impact on a surface only, the coefficient simplifies to be equal to 1.2. Using this method, the coefficients in the mean dynamic pressure equation defining $C_p^{'}$ are replaced by the 1.2 multiplier.

For close-ended cracks the pressure forces on the rock mass could be increased significantly caused by hydrodynamic pressure fluctuations of the fluid in the crack. In this case, the fluctuating dynamic pressure coefficient could be increased by 4 times.

The final method for determining removal of rock due to uplift is similar to the key block theory where the removal of blocks is affected by their relationship to other rock blocks in the area. The equation for determining uplift, h_{up}, of a rock block from a rock formation [3, 4, 10] is:

$$h_{up} = \left[\frac{2(x_b + 2z_b)}{c}\right]^2 \frac{1}{2g \cdot x_b^4 \cdot z_b^2 \cdot \rho_s^2}\left[C_I \cdot \varphi \cdot \gamma \cdot \frac{V_j^2}{2g} \cdot x_b^2 - (\gamma_s - \gamma) \cdot x_b^2 \cdot z_b - F_{sh}\right]^2$$

where c is the pressure wave celerity, ρ, γ are the density and unit weights of the material or water, F_{sh} is the shear force on the sides of the crack and assumed to be zero, and x_b, z_b are the sides and height of the rock block, respectively. If the ratio of the uplift over the height of a rock block is greater than 1 or less than 0.1 the block will or will be removed from the formation. The celerity may be varied from 1115.5 to 3280.8 ft/s to look at sensitivity [10].

Given the locations of the jet impingement at Yellowtail Dam, the pressure magnitudes caused by jet impact on the rock surfaces or exposed joints might be needed. No requests for further pressure force computations were made during the risk assessment.

Stream Power and Rock Erodibility

Figures 9 and 10 show the predicted footprint of the overtopping jets for the various flow rates investigated where they would impinge on the rock abutments and the downstream face of the dam. The methodology used to determine if the abutment rock will erode producing a mode of failure for the dam is a function of the erosive power of the water and the quality and structure of the rock as determined by Annandale [10].

Rock Erodibility

The erodibility index is a geomechanical index that is used to quantify the relative ability of earth and engineered earth materials to resist the erosive capacity of water [10].

Five factors are considered in the erodibility index:

M_s: Material strength or Mass strength	Range 0.45-250
K_b: Block Size RQD/J_n	Range J_n 1-5; RQD 0-100 i.e. 0-100
K_d: Shear strength of joints J_r/J_a	Range J_r 1-4; J_a 0.75-18 i.e. 0.2-18
J_s: Relative ground structure number	Range 0.37-1.00

The overall erodibility index, K, is the product of these four factors. All of these factors are important; however, this method may not distribute the appropriate proportion of each component to the overall factor in a way that is consistent with rock mechanics and the stability in rock masses. Based on the ranges of values for these factors it is easy to see that the two dominant factors, M_s and K_b, are arguably over-valued given the range of expected values up to 250 for M_s and up to 100 for the RQD. In most stability problems encountered thus far at Reclamation dam sites involving rock masses, it is the joint orientations relative to the free face, the direction of the load, and the shear strength of

the joints, that are often dominant parameters. The factors K_d and J_s address these features better in the typical rock masses and; therefore, should carry the most weight for the hard rock condition at Yellowtail and at most Reclamation concrete dam sites. However, the maximum suggested range for these values in 2 orders of magnitude less than those suggested for the M_s and K_b. In addition, these rock features are not handled in a 3-D framework, nor does the method developed by Annandale [10] address the concept of removal of rock block. These can potentially be serious shortcomings when developing the erodibility index for rock abutments. Also, the empirical line defining the boundary between erosion and no erosion, as a function of the stream power and erodibility index, is dominated by data from low energy stream power conditions on weak soil-lined channels. This line might; therefore, apply best to conditions that are dominated by the mass strength factor, M_s. In most cases for plunge pools and concrete dam abutments, the mass strength factor could be considered constant because most are founded in hard rock formations at the high end of the strength range [7, 8, 9].

This does not mean that we cannot estimate the erosion potential at Yellowtail Dam. The erodibility indices for the abutments at Yellowtail Dam will be developed during the June 2009 risk assessment if determined necessary to evaluate the potential risk due to overtopping and rock erosion.

Stream Power

The stream power is the rate at which energy is applied after the jet has travelled through a vertical distance, Z, to the point of impingement on a surface or plunge point in a pool:

$$P_{jet} = \gamma Q Z$$

where P_{jet} is the total stream power of the jet, γ is the unit weight of water, and Q is the total discharge. The stream power per unit area is determined by dividing the total stream power by the footprint of the area of the jet at the point of impact. This stream power per unit area of the jet is defined as:

$$p_{jet} = \frac{\gamma Q Z}{A_i}$$

and may be used to determine whether erosion will occur or not as a function of the erodibility of the material or rock. The unit area of the jet changes with the fall both above and below the tailwater and is based upon the characteristics of the jet, including the spread and angle of jet impingement and in this case, the vertical fall to jet break up. The stream power density for the 2 though 18 feet of overtopping heads investigated are shown in appendix B on table B1. The stream power density was assumed to not increase after the jet break up occurred because the jet core, thus remaining solid water mass was assumed to be dissipated.

Figure 11 shows the stream power density as a function of elevation from the data in Appendix B on table B1. The figure shows the increase in stream power density as the jet falls through the air until the jet core is broken up. Once the core is broken up, it is assumed that the stream power density would be constant with further fall of the jet and

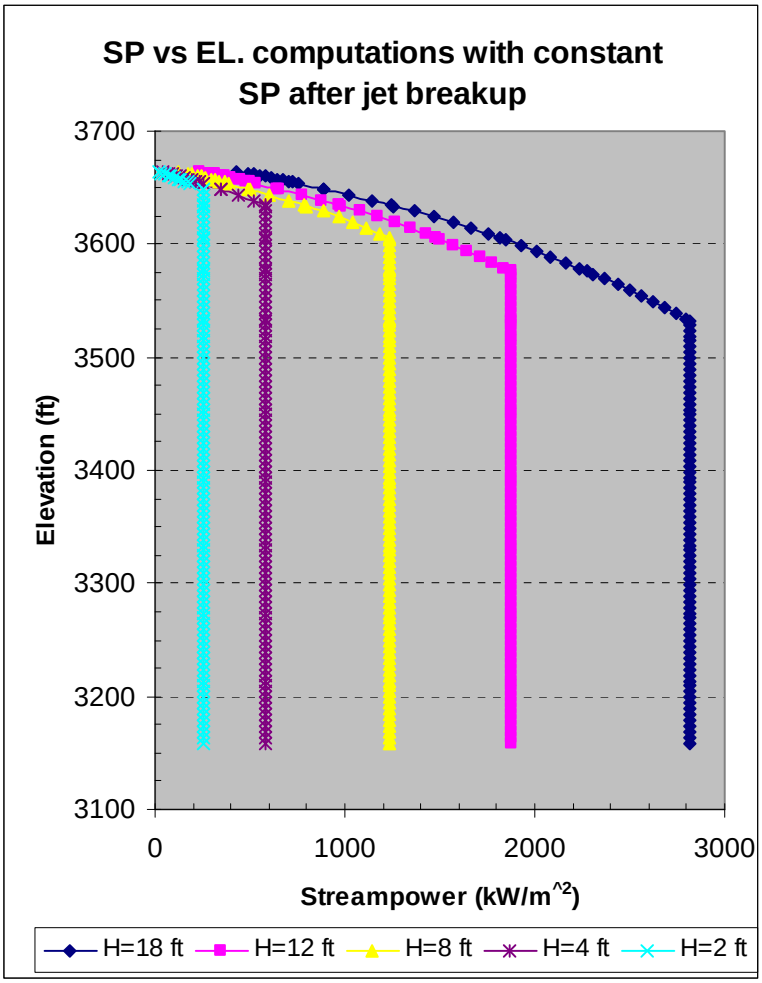

Figure 11. - Stream power density per unit area available versus elevation as the jets travel from the downstream parapet on the dam.

equal to the values shown in the last row of table B1. This could potentially not be a conservative result if the water would to coalesce again during the fall; however, at this time, the assumption of no increase in stream power density after jet break up seems physically to make sense.

Table 8 shows the minimum and maximum stream power densities for the range of investigated overtopping heads with the traditional range of potential material erodibility indices from the stream power versus erodibility index graph from Annandale [10].

Table 8. - Minimum and maximum stream power densities computed for the overtopping heads investigated assuming material erodibility over the typical range.

Stream Power	K	Overtopping Head (ft)

(kW/m^2)		18	12	8	4	2
Minimum	0.1	427	232	127	45	16
Maximum	100000	2820	1876	1232	579	260

There is a limit or threshold of erosion based upon a body of empirical data [10]. A threshold of erodibility has been defined as a function of the erodibility index, K as follows [10]:

$$P_c = K^{0.75} \qquad \text{For higher erodibility (K>0.1)}$$

$$P_c = 0.48K^{0.44} \text{ For less erodibility (K<0.1)}$$

The threshold stream power densities were computed for Yellowtail Dam, assuming that K > 0.1 for the hard rock masses present over most of the abutment area. There is a 50 percent probability that erosion will occur for conditions exceeding the "erosion threshold" developed by Annandale [10] based upon the available data at the time.

Figure 12 shows the typical graph of erodibility of material versus stream power density with the expected minimum and maximum stream power densities for the various overtopping heads investigated over the range of material erodibility usually plotted.

Figure 12 shows the typical graph of erodibility versus stream power density with the threshold values from table 8 are plotted with assumed minimum and maximum potential erodibility factors computed and shown in table 8.

Figure 12 shows that the majority of the stream power density available due to the fall of the jets plots above the critical threshold for erosion to occur over the range of erodibility indices shown. This does not mean that, when computed, the erodibility indices for Yellowtail Dam will not be large enough to be in the zone of no erosion. Also, if it is assumed, ultimately conservatively that the jet core remains in tact and the jet width would continue increasing, then the stream power density would also increase. Erosion caused by a jet that is assumed to have an in tact core might then become a factor depending upon the quality of the rock.

Figures 9, 10, 11 and 12 were used in the risk assessment to assign probability of abutment erosion during overtopping. In addition, stream power densities were roughly developed during the risk assessment for flow overtopping portions of the dam that would then cause flow down the groin of the dam. These values for stream power and the rough erodibility indices for the upper breccia and the lower limestone rock that were also developed during the risk meeting are given in table 9.

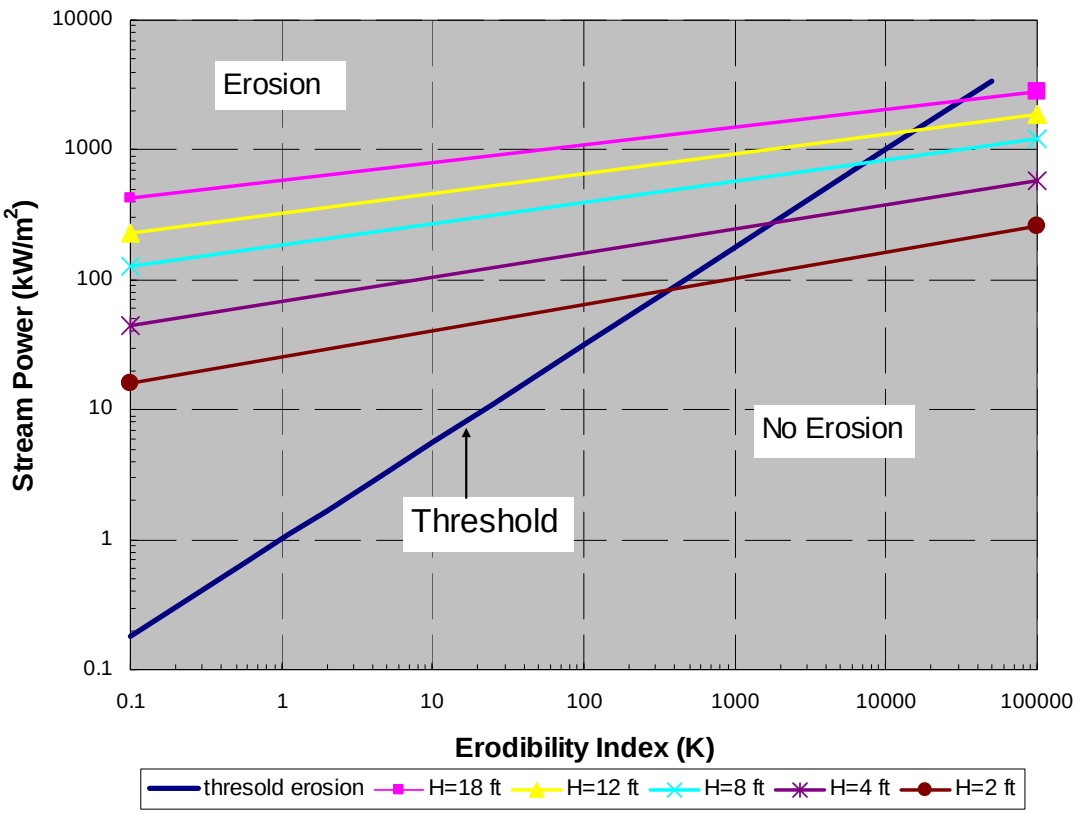

Figure 12. - Stream power density versus threshold stream power density where erosion would be considered likely above the line and no erosion below the line. Minimum and maximum stream power densities were plotted over the range of erodibility indices that are generally considered attainable for materials.

Table 9. - Stream power and erodibility indices for overtopping flows and surface flows with erodibility indices for the breccia and limestone developed during the risk assessment.

Overtopping Depth (OT) (feet)	Breccia		Limestone	
	Stream Power	Erosion Index	Stream Power	Erosion Index
4	580	750	200	2300
10	1554	750	650	2300
18	2820	750	1400	2300

Additional statistical analyses have been performed by Wibowo, et al [21] on the prototype data points from Annandale [10] and additional data [22]. The threshold line determined by Annandale [10] for the occurrence or non-occurrence of erosion was determined to be the line of a 50 percent probability of erosion and slightly adjusted. In addition, the 1 and 99 percent probability of erosion were computed for the data set and

added onto the chart with the new data set for use in predicting above the 50 percent line and no erosion predicted below the line. This new chart of erosion prediction was used during the risk assessment with the data from table 9 to determine the probability of abutment erosion. Figure 13 shows a plot of the values determined during the risk assessment as an update to the original work shown in figure 12. It appears likely that the breccia material will erode while the limestone will be quite resistant to erosion. The risk assessment documentation will provide the final probability of erosion [23].

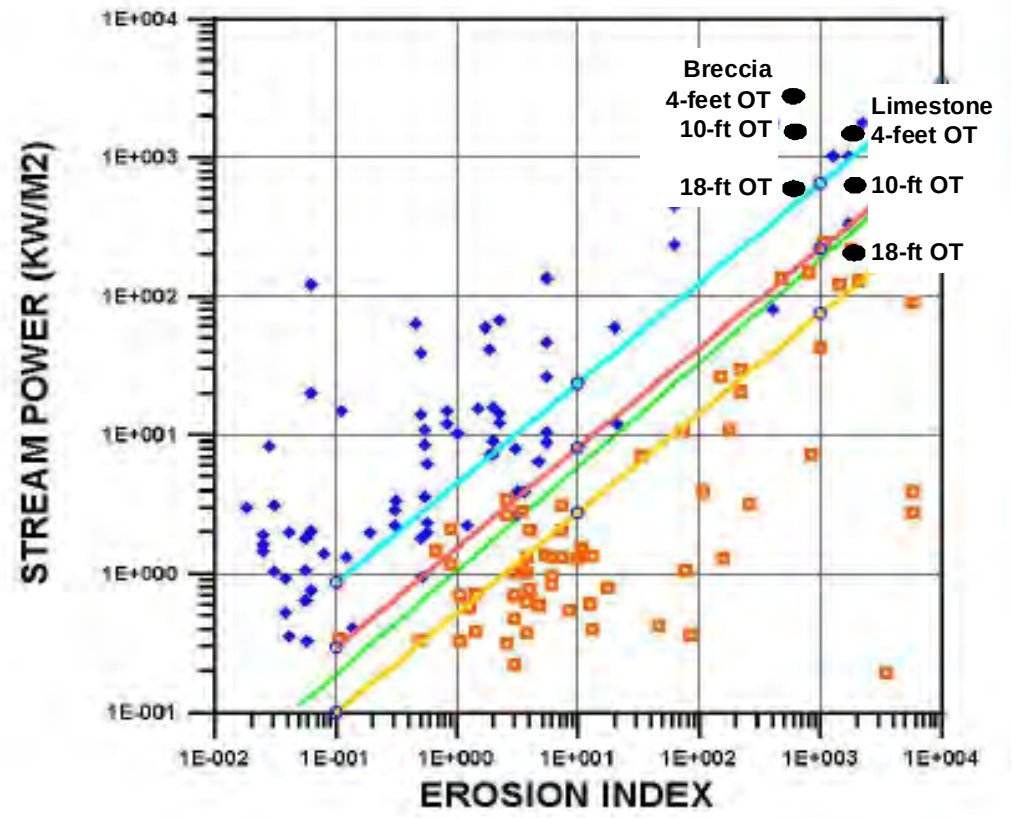

Figure 13. - Stream power density versus the erodibility index for the breccia and limestone rock at Yellowtail Dam. The probability of erosion is represented by the upper blue line at 99 percent, the middle lines at 50 percent, and the lower orange line at 1 percent.

Conclusions

The following conclusions were drawn from analysis of the range of overtopping heads and flows investigated:

- The analysis of the jet characteristics was conducted with both circular and rectangular jet methodologies because previous overtopping analyses had been performed with circular jet equations converted to rectangular area. It was concluded that an overtopping jet is more similar to a rectangular shape than circular, thus newly published experimentally based rectangular jet equations were used in this analysis [6].
- The overtopping jet for small 2 and 4 ft overtopping heads will impinge on the face of the dam. The trajectories for 8 and 12-ft overtopping will impinge up high on the abutments and on the power plant below. The 18-ft overtopping will impinge upon the rock abutments along the junction with the foundation of the dam and onto the power plant at the toe of the dam. Figures 9 and 10 show the impingement locations. With this locations determined, the type and jointing of the rock exposed to the overtopping jet and flow may be determined in the risk assessment.
- The jet will initially contract, spread, and break up, leading to dissipation of the jet core. Table 5 shows that all the jets will break up at some elevation.
- Engineering judgment is still required to interpret the results of the presented analyzes due to uncertainties associated with the jet characteristics and the accompanying assumptions made. Conclusions were drawn from figure 13 during the risk assessment and are documented in TM No. YEL-8013-RA-2009-1.

Recommendations

The first step in determining the erodibility of a material is to define the jet characteristics at the point of impingement or contact with the material surface. If the jet characteristics are not well defined then the use of the stream power analysis is also questionable because it is based upon the area of the jet or flow. Jet characteristic need to be defined using large-scale research facilities where the free-falling jet would not be subjected to scale effects while aerating throughout the fall. Once jet characteristics are defined and questions answered regarding the jet properties during the fall, then application of the stream power density could be done with more certainty.

Application of the erodibility index analysis in rock is potentially inappropriate because of the way the theory was initially developed. The erodibility index is developed from weighted material properties developed primarily from soil materials. The physical mechanisms for erosion for these two situations are entirely different. The rock erodibility indices need verification through the use of extensive prototype mapping of rock features in a prototype installation prior to and after controlled releases. This might take an effort to locate sites where flow could be expected within a reasonable amount of time, unlike most Reclamation sites where large releases are rare.

References

[1] "Yellowtail Dam and Yellowtail Afterbay Dam, Comprehensive Facility Review," prepared by Marijo Camrud and Dan Levish, Bureau of Reclamation, Denver, Colorado, April, 2002.

[2] Ervine and Falvey, 1987, "Behaviour of turbulent water jets in the atmosphere and in plunge pools," Proceedings Institution of Civil Engineers, Part 2, Volume 83, pp. 295-314.

[3] Ervine, D.A., et al, 1997, "Pressure Fluctuations on Plunge Pool Floors," Journal of Hydraulic Research, Vol. 35, No. 2, pp. 257-279.

[4] Bollaert, Erik, 2002, "Transient water pressures in joints and formation of rock scour due to high-velocity jet impact," Communication 13, Laboratoire de Constructions Hydrauliques Ecole Polytechnique Federale de Lausanne, Edited by Professor Dr. A. Schleiss, Lausanne, Switzerland, 2002.

[5] Wahl, T.L., Frizell, K.H., Cohen, E.A., "Computing the Trajectory of Free Jets," ASCE Journal of Hydraulic Engineering, Technical Note, Volume 134, Number 2, February 2008.

[6] Castillo, Luis, G., "Aerated jets and Pressure Fluctuation in Plunge Pools," Proceedings, 7th International Conference on HydroScience and Engineering, Philadelphia, Pennsylvania, Drexel University, ISBN:0977447405, September 10-13, 2006.

[7] Frizell, K. H., "Hydraulic Investigations of the Erosion Potential of Flows Overtopping Gibson Dam, Sun River Project, Montana, Great Plains Region, HL-2006-02," U. S. Department of Interior, Bureau of Reclamation, Technical Services Center, Denver, Colorado, April 2006.

[8] Frizell, K. H., "Hydraulic Investigations of the Erosion Potential of Flows Overtopping Owyhee Dam, Owyhee Project, Oregon-Idaho, Pacific Northwest Region, PAP-956," U. S. Department of Interior, Bureau of Reclamation, Technical Services Center, Denver, Colorado, July 2006.

[9] Frizell, K. H., "Analysis of the Erosion Potential of Flow Overtopping Arrowrock Dam, Boise Project, Idaho, Snake River Office, Pacific Northwest Region, TM-ARR-8560-IE-2007-1," U. S. Department of Interior, Bureau of Reclamation, Technical Services Center, Denver, Colorado, April 2007.

[10] Annandale, George W., 2006, "Scour Technology Mechanics and Engineering Practice," McGraw-Hill Civil Engineering Series, ISBN 0-07-144057-7.

[11] Wahl, Tony L., "Jet Erosion Tests of Breccia Core Samples from Yellowtail Dam, Draft" U.S. Department of Interior, Bureau of Reclamation, Technical Services Center, Denver, Colorado, March 2009.

[12] Final Construction Engineering Geology Report, Yellowtail Dam and Power plant, Hardin Unit, Montana, Missouri Basin Project, April 1966.

[13] "Yellowtail Dam Issue Evaluation – Geology for Foundation Stability Analysis and Block Evaluation - Phase 1", *Technical Memorandum Number YT-8320-01*, Bureau of Reclamation, Denver, Colorado, and Pick-Sloan Missouri Basin Project, Great Plains Region, Billings, Montana. August, 2006.

[14] "Yellowtail Dam Issue Evaluation Phase 2- Upper Left Abutment Geology for Foundation Stability Analysis and Karst Breccia Evaluation, Draft," Technical Memorandum Number YT- 86-68320-2009-04, U. S. Department of Interior, Bureau of Reclamation, Technical Services Center, Denver, Colorado, 2009.

[15] Technical Memorandum No. YT-86-68312-2009-1, "Yellowtail Dam Issue Evaluation Static and Dynamic Foundation Analyses, Draft," U. S. Department of Interior, Bureau of Reclamation, Technical Services Center, Denver, Colorado, 2009.

[16] "Assessment of the Hydrologic/Hydrauilic Loading Conditions, Yellowtail Dam and Afterbay, Pick-Sloan Missouri Basin Project, Great Plains Region," TM No. YEL-8130-IE-2009-1, U. S. Department of Interior, Bureau of Reclamation, Technical Services Center, Denver, Colorado, May 2009.

[17] "Yellowtail Dam and Yellowtail Afterbay Dam, Hydrologic Hazard," Flood Hydrology Group, Bureau of Reclamation, Denver, Colorado, June, 2007.

[18] "Probable Maximum Flood Study, Yellowtail Dam, Missouri River Basin, Montana", Memorandum to Regional Director, Billings, Montana, Bureau of Reclamation, Denver, CO, July 18, 1988.

[19] Chow, Ven Te, "Open-Channel Hydraulic," McGraw-Hill, Inc., 1959.

[20] Rouse, H. R., 1936, "Discharge Characteristics of the Free Overfall," Civil Engineering, Vol. 6, No. 4.

[21] Wibowo, J.L., D.E. Yule, and E. Villanueva, "Earth and Rock Surface Spillway Erosion Risk Assessment," Proceedings, 40th U.S. Symposium on Rock Mechanics, Anchorage Alaska, 2005.

[22] Wibowo, J.L., and W.L. Murphy. 2005. Unlined spillway erosion prediction model. USACE ERDC Technical Report, Vicksburg, MS.

[23] "Yellowtail Dam Issue Evaluation - Risk Analysis," TM No. YEL-8013-RA-2009-1, U. S. Department of Interior, Bureau of Reclamation, Technical Services Center, Denver, Colorado, 2009.

Appendix A

Jet Trajectories for 18, 12, 8 4 and 2 ft of reservoir overtopping heads.

Table A1. - Trajectory locations for a reservoir head of 18 ft horizontal and drop (z) distances and elevations from the downstream parapet location. The trajectories include the spread of the jet due to gravity and turbulence.

Drop z ft	El. Lower nappe ft	Lower nappe distance from d/s parapet ft	Upper nappe distance from d/s parapet ft	El. Upper nappe ft	Jet width Bj ft
0	3664	0.00	0.00	3671.71	7.71
-1	3663	5.85	7.14	3670.71	7.02
-2	3662	8.50	9.87	3669.71	6.97
-3	3661	10.52	11.98	3668.71	6.92
-4	3660	12.21	13.76	3667.71	6.89
-5	3659	13.70	15.34	3666.71	6.85
-6	3658	15.05	16.77	3665.71	6.83
-7	3657	16.28	18.08	3664.71	6.81
-8	3656	17.43	19.31	3663.71	6.79
-9	3655	18.50	20.46	3662.71	6.78
-10	3654	19.52	21.56	3661.71	6.77
-14.64	3649.36	23.66	26.04	3657.07	6.76
-15	3649	23.95	26.35	3656.71	6.76
-20	3644	27.67	30.42	3651.71	6.81
-25	3639	30.94	34.00	3646.71	6.88
-29.27	3634.73	33.47	36.79	3642.44	6.96
-30	3634	33.89	37.25	3641.71	6.98
-35	3629	36.60	40.24	3636.71	7.09
-40	3624	39.11	43.03	3631.71	7.21
-45	3619	41.47	45.65	3626.71	7.33
-50	3614	43.70	48.14	3621.71	7.47
-55	3609	45.83	50.50	3616.71	7.60
-58.55	3605.45	47.27	52.11	3613.16	7.70
-60	3604	47.85	52.76	3611.71	7.74
-65	3599	49.79	54.92	3606.71	7.88
-70	3594	51.66	57.01	3601.71	8.02
-75	3589	53.46	59.02	3596.71	8.16
-80	3584	55.20	60.97	3591.71	8.30
-85	3579	56.89	62.86	3586.71	8.44
-87.82	3576.18	57.82	63.90	3583.89	8.52
-90	3574	58.52	64.69	3581.71	8.58
-95	3569	60.12	66.48	3576.71	8.72
-100	3564	61.67	68.22	3571.71	8.86
-105	3559	63.18	69.91	3566.71	8.99
-110	3554	64.65	71.57	3561.71	9.13
-115	3549	66.09	73.19	3556.71	9.26
-120	3544	67.51	74.77	3551.71	9.40
-125	3539	68.89	76.33	3546.71	9.53
-130	3534	70.24	77.85	3541.71	9.66
-131.73	3532.27	70.70	78.37	3539.98	9.71
-135	3529	71.57	79.34	3536.71	9.80

Drop z ft	El. Lower nappe ft	Lower nappe distance from d/s parapet ft	Upper nappe distance from d/s parapet ft	El. Upper nappe ft	Jet width Bj ft
-140	3524	72.87	80.81	3531.71	9.93
-145	3519	74.15	82.25	3526.71	10.05
-150	3514	75.41	83.66	3521.71	10.18
-155	3509	76.65	85.05	3516.71	10.31
-160	3504	77.87	86.42	3511.71	10.44
-165	3499	79.06	87.77	3506.71	10.56
-170	3494	80.24	89.10	3501.71	10.68
-175	3489	81.41	90.41	3496.71	10.81
-180	3484	82.55	91.70	3491.71	10.93
-185	3479	83.68	92.98	3486.71	11.05
-190	3474	84.80	94.23	3481.71	11.17
-195	3469	85.90	95.47	3476.71	11.29
-200	3464	86.98	96.70	3471.71	11.41
-205	3459	88.06	97.91	3466.71	11.53
-210	3454	89.12	99.10	3461.71	11.64
-215	3449	90.16	100.28	3456.71	11.76
-220	3444	91.20	101.45	3451.71	11.87
-225	3439	92.22	102.60	3446.71	11.99
-230	3434	93.23	103.74	3441.71	12.10
-235	3429	94.23	104.87	3436.71	12.21
-240	3424	95.22	105.99	3431.71	12.32
-245	3419	96.20	107.09	3426.71	12.43
-250	3414	97.17	108.19	3421.71	12.54
-255	3409	98.13	109.27	3416.71	12.65
-260	3404	99.09	110.34	3411.71	12.76
-265	3399	100.03	111.41	3406.71	12.87
-270	3394	100.96	112.46	3401.71	12.97
-275	3389	101.88	113.50	3396.71	13.08
-280	3384	102.80	114.54	3391.71	13.19
-285	3379	103.71	115.56	3386.71	13.29
-290	3374	104.61	116.58	3381.71	13.40
-295	3369	105.50	117.58	3376.71	13.50
-300	3364	106.38	118.58	3371.71	13.60
-305	3359	107.26	119.57	3366.71	13.70
-310	3354	108.13	120.55	3361.71	13.81
-315	3349	108.99	121.53	3356.71	13.91
-320	3344	109.85	122.49	3351.71	14.01
-325	3339	110.70	123.45	3346.71	14.11
-330	3334	111.54	124.40	3341.71	14.21
-335	3329	112.38	125.35	3336.71	14.30
-340	3324	113.21	126.29	3331.71	14.40
-345	3319	114.03	127.22	3326.71	14.50
-350	3314	114.85	128.14	3321.71	14.60
-355	3309	115.66	129.06	3316.71	14.69
-360	3304	116.47	129.97	3311.71	14.79

Drop z ft	El. Lower nappe ft	Lower nappe distance from d/s parapet ft	Upper nappe distance from d/s parapet ft	El. Upper nappe ft	Jet width Bj ft
-365	3299	117.27	130.87	3306.71	14.89
-370	3294	118.06	131.77	3301.71	14.98
-375	3289	118.85	132.66	3296.71	15.07
-380	3284	119.64	133.55	3291.71	15.17
-385	3279	120.42	134.43	3286.71	15.26
-390	3274	121.19	135.31	3281.71	15.35
-395	3269	121.96	136.18	3276.71	15.45
-400	3264	122.73	137.04	3271.71	15.54
-405	3259	123.48	137.90	3266.71	15.63
-410	3254	124.24	138.75	3261.71	15.72
-415	3249	124.99	139.60	3256.71	15.81
-420	3244	125.74	140.44	3251.71	15.90
-425	3239	126.48	141.28	3246.71	15.99
-430	3234	127.22	142.11	3241.71	16.08
-435	3229	127.95	142.94	3236.71	16.17
-440	3224	128.68	143.77	3231.71	16.26
-445	3219	129.40	144.59	3226.71	16.35
-450	3214	130.12	145.40	3221.71	16.43
-455	3209	130.84	146.21	3216.71	16.52
-460	3204	131.55	147.02	3211.71	16.61
-465	3199	132.26	147.82	3206.71	16.70
-470	3194	132.97	148.61	3201.71	16.78
-475	3189	133.67	149.41	3196.71	16.87
-480	3184	134.36	150.19	3191.71	16.95
-485	3179	135.06	150.98	3186.71	17.04
-490	3174	135.75	151.76	3181.71	17.12
-495	3169	136.43	152.54	3176.71	17.21
-500	3164	137.12	153.31	3171.71	17.29
-505	3159	137.80	154.08	3166.71	17.37
-510	3154	138.47	154.84	3161.71	17.46
-515	3149	139.15	155.60	3156.71	17.54
-520	3144	139.82	156.36	3151.71	17.62
-525	3139	140.48	157.11	3146.71	17.70
-530	3134	141.15	157.86	3141.71	17.79
-535	3129	141.81	158.61	3136.71	17.87
-540	3124	142.47	159.35	3131.71	17.95
-545	3119	143.12	160.09	3126.71	18.03
-550	3114	143.77	160.83	3121.71	18.11

Table A2. - Trajectory locations for a reservoir head of 12 ft horizontal and drop (z) distances and elevations from the downstream parapet location. The trajectories include the spread of the jet due to gravity and turbulence.

Drop z ft	El. Lower nappe ft	Lower nappe distance from d/s parapet ft	Upper nappe distance from d/s parapet ft	El. Upper nappe ft	Jet width B_j ft
0	3664	0.00	0.00	3669.14	5.14
-1	3663	4.96	5.64	3668.14	4.46
-2	3662	7.12	7.87	3667.14	4.39
-3	3661	8.78	9.59	3666.14	4.34
-4	3660	10.16	11.05	3665.14	4.29
-5	3659	11.38	12.33	3664.14	4.25
-6	3658	12.49	13.49	3663.14	4.22
-7	3657	13.50	14.56	3662.14	4.19
-8	3656	14.44	15.56	3661.14	4.17
-9	3655	15.32	16.50	3660.14	4.15
-10	3654	16.15	17.38	3659.14	4.14
-14.64	3649.36	19.55	21.03	3654.50	4.11
-15	3649	19.79	21.28	3654.14	4.11
-20	3644	22.85	24.58	3649.14	4.13
-25	3639	25.54	27.48	3644.14	4.18
-29.27	3634.73	27.63	29.75	3639.87	4.24
-30	3634	27.97	30.12	3639.14	4.25
-35	3629	30.20	32.54	3634.14	4.32
-40	3624	32.28	34.79	3629.14	4.41
-45	3619	34.22	36.92	3624.14	4.50
-50	3614	36.07	38.92	3619.14	4.59
-55	3609	37.82	40.83	3614.14	4.68
-58.55	3605.45	39.01	42.13	3610.59	4.75
-60	3604	39.49	42.66	3609.14	4.77
-65	3599	41.09	44.41	3604.14	4.87
-70	3594	42.63	46.09	3599.14	4.96
-75	3589	44.12	47.72	3594.14	5.06
-80	3584	45.56	49.29	3589.14	5.15
-85	3579	46.96	50.82	3584.14	5.24
-87.82	3576.18	47.72	51.66	3581.32	5.30
-90	3574	48.31	52.30	3579.14	5.34
-95	3569	49.62	53.74	3574.14	5.43
-100	3564	50.91	55.14	3569.14	5.52
-105	3559	52.16	56.51	3564.14	5.61
-110	3554	53.38	57.85	3559.14	5.70
-115	3549	54.57	59.15	3554.14	5.79
-120	3544	55.74	60.43	3549.14	5.88
-125	3539	56.88	61.69	3544.14	5.97
-130	3534	58.00	62.91	3539.14	6.06
-131.73	3532.27	58.38	63.33	3537.41	6.09

Drop z ft	El. Lower nappe ft	Lower nappe distance from d/s parapet ft	Upper nappe distance from d/s parapet ft	El. Upper nappe ft	Jet width B_j ft
-135	3529	59.10	64.12	3534.14	6.14
-140	3524	60.18	65.30	3529.14	6.23
-145	3519	61.24	66.46	3524.14	6.31
-150	3514	62.28	67.61	3519.14	6.40
-155	3509	63.30	68.73	3514.14	6.48
-160	3504	64.31	69.83	3509.14	6.56
-165	3499	65.30	70.92	3504.14	6.65
-170	3494	66.28	71.99	3499.14	6.73
-175	3489	67.24	73.05	3494.14	6.81
-180	3484	68.19	74.09	3489.14	6.89
-185	3479	69.12	75.12	3484.14	6.96
-190	3474	70.05	76.13	3479.14	7.04
-195	3469	70.96	77.13	3474.14	7.12
-200	3464	71.86	78.12	3469.14	7.20
-205	3459	72.75	79.09	3464.14	7.27
-210	3454	73.62	80.06	3459.14	7.35
-215	3449	74.49	81.01	3454.14	7.42
-220	3444	75.35	81.95	3449.14	7.50
-225	3439	76.19	82.88	3444.14	7.57
-230	3434	77.03	83.80	3439.14	7.64
-235	3429	77.86	84.71	3434.14	7.72
-240	3424	78.68	85.61	3429.14	7.79
-245	3419	79.49	86.50	3424.14	7.86
-250	3414	80.29	87.38	3419.14	7.93
-255	3409	81.09	88.26	3414.14	8.00
-260	3404	81.88	89.12	3409.14	8.07
-265	3399	82.66	89.98	3404.14	8.14
-270	3394	83.43	90.83	3399.14	8.21
-275	3389	84.19	91.67	3394.14	8.28
-280	3384	84.95	92.50	3389.14	8.35
-285	3379	85.70	93.33	3384.14	8.41
-290	3374	86.45	94.15	3379.14	8.48
-295	3369	87.19	94.96	3374.14	8.55
-300	3364	87.92	95.76	3369.14	8.61
-305	3359	88.65	96.56	3364.14	8.68
-310	3354	89.37	97.35	3359.14	8.74
-315	3349	90.08	98.14	3354.14	8.81
-320	3344	90.79	98.92	3349.14	8.87
-325	3339	91.49	99.69	3344.14	8.94
-330	3334	92.19	100.46	3339.14	9.00
-335	3329	92.88	101.22	3334.14	9.06
-340	3324	93.57	101.97	3329.14	9.13
-345	3319	94.25	102.72	3324.14	9.19
-350	3314	94.93	103.47	3319.14	9.25
-355	3309	95.60	104.21	3314.14	9.31

Drop z ft	El. Lower nappe ft	Lower nappe distance from d/s parapet ft	Upper nappe distance from d/s parapet ft	El. Upper nappe ft	Jet width B_j ft
-360	3304	96.27	104.94	3309.14	9.37
-365	3299	96.94	105.67	3304.14	9.44
-370	3294	97.59	106.39	3299.14	9.50
-375	3289	98.25	107.11	3294.14	9.56
-380	3284	98.90	107.83	3289.14	9.62
-385	3279	99.54	108.54	3284.14	9.68
-390	3274	100.19	109.24	3279.14	9.74
-395	3269	100.82	109.94	3274.14	9.80
-400	3264	101.46	110.64	3269.14	9.85
-405	3259	102.09	111.33	3264.14	9.91
-410	3254	102.71	112.02	3259.14	9.97
-415	3249	103.33	112.70	3254.14	10.03
-420	3244	103.95	113.38	3249.14	10.09
-425	3239	104.57	114.06	3244.14	10.14
-430	3234	105.18	114.73	3239.14	10.20
-435	3229	105.78	115.40	3234.14	10.26
-440	3224	106.39	116.06	3229.14	10.31
-445	3219	106.99	116.72	3224.14	10.37
-450	3214	107.59	117.38	3219.14	10.43
-455	3209	108.18	118.03	3214.14	10.48
-460	3204	108.77	118.68	3209.14	10.54
-465	3199	109.36	119.33	3204.14	10.59
-470	3194	109.94	119.97	3199.14	10.65
-475	3189	110.52	120.61	3194.14	10.70
-480	3184	111.10	121.24	3189.14	10.76
-485	3179	111.67	121.87	3184.14	10.81
-490	3174	112.25	122.50	3179.14	10.86
-495	3169	112.82	123.13	3174.14	10.92
-500	3164	113.38	123.75	3169.14	10.97
-505	3159	113.94	124.37	3164.14	11.02
-510	3154	114.51	124.99	3159.14	11.08
-515	3149	115.06	125.60	3154.14	11.13
-520	3144	115.62	126.21	3149.14	11.18
-525	3139	116.17	126.82	3144.14	11.24
-530	3134	116.72	127.42	3139.14	11.29
-535	3129	117.27	128.02	3134.14	11.34
-540	3124	117.81	128.62	3129.14	11.39
-545	3119	118.35	129.22	3124.14	11.44
-550	3114	118.89	129.81	3119.14	11.49

Table A3. - Trajectory locations for a reservoir head of 8 ft horizontal and drop (z) distances and elevations from the downstream parapet location. The trajectories include the spread of the jet due to gravity and turbulence.

Drop z ft	El. Lower nappe ft	Lower nappe distance from d/s parapet ft	Upper nappe distance from d/s parapet ft	El. Upper nappe ft	Jet width Bj ft
0	3664	0.00	0.00	3667.43	3.43
-1	3663	4.15	4.51	3666.43	2.84
-2	3662	5.91	6.33	3665.43	2.76
-3	3661	7.26	7.73	3664.43	2.71
-4	3660	8.40	8.92	3663.43	2.66
-5	3659	9.40	9.96	3662.43	2.62
-6	3658	10.30	10.91	3661.43	2.59
-7	3657	11.13	11.78	3660.43	2.56
-8	3656	11.90	12.59	3659.43	2.54
-9	3655	12.62	13.35	3658.43	2.53
-10	3654	13.31	14.07	3657.43	2.51
-14.64	3649.36	16.10	17.03	3652.79	2.49
-15	3649	16.30	17.24	3652.43	2.49
-20	3644	18.81	19.91	3647.43	2.50
-25	3639	21.02	22.27	3642.43	2.54
-29.27	3634.73	22.74	24.10	3638.16	2.58
-30	3634	23.02	24.40	3637.43	2.58
-35	3629	24.86	26.37	3632.43	2.64
-40	3624	26.57	28.19	3627.43	2.70
-45	3619	28.17	29.91	3622.43	2.76
-50	3614	29.69	31.54	3617.43	2.82
-55	3609	31.13	33.08	3612.43	2.88
-58.55	3605.45	32.12	34.14	3608.88	2.93
-60	3604	32.51	34.56	3607.43	2.95
-65	3599	33.83	35.98	3602.43	3.01
-70	3594	35.11	37.34	3597.43	3.07
-75	3589	36.33	38.66	3592.43	3.14
-80	3584	37.52	39.93	3587.43	3.20
-85	3579	38.67	41.16	3582.43	3.26
-87.82	3576.18	39.30	41.84	3579.61	3.30
-90	3574	39.78	42.36	3577.43	3.33
-95	3569	40.87	43.53	3572.43	3.39
-100	3564	41.93	44.66	3567.43	3.45
-105	3559	42.96	45.77	3562.43	3.51
-110	3554	43.96	46.85	3557.43	3.57
-115	3549	44.95	47.91	3552.43	3.63
-120	3544	45.91	48.94	3547.43	3.68
-125	3539	46.85	49.95	3542.43	3.74
-130	3534	47.78	50.95	3537.43	3.80
-131.73	3532.27	48.09	51.29	3535.70	3.82
-135	3529	48.69	51.92	3532.43	3.86

Drop z ft	El. Lower nappe ft	Lower nappe distance from d/s parapet ft	Upper nappe distance from d/s parapet ft	El. Upper nappe ft	Jet width Bj ft
-140	3524	49.58	52.88	3527.43	3.91
-145	3519	50.45	53.82	3522.43	3.97
-150	3514	51.31	54.74	3517.43	4.02
-155	3509	52.15	55.65	3512.43	4.08
-160	3504	52.98	56.54	3507.43	4.13
-165	3499	53.80	57.42	3502.43	4.18
-170	3494	54.61	58.29	3497.43	4.23
-175	3489	55.40	59.14	3492.43	4.29
-180	3484	56.19	59.98	3487.43	4.34
-185	3479	56.96	60.81	3482.43	4.39
-190	3474	57.72	61.63	3477.43	4.44
-195	3469	58.47	62.44	3472.43	4.49
-200	3464	59.21	63.24	3467.43	4.54
-205	3459	59.95	64.03	3462.43	4.59
-210	3454	60.67	64.81	3457.43	4.64
-215	3449	61.39	65.58	3452.43	4.68
-220	3444	62.09	66.34	3447.43	4.73
-225	3439	62.79	67.09	3442.43	4.78
-230	3434	63.49	67.83	3437.43	4.83
-235	3429	64.17	68.57	3432.43	4.87
-240	3424	64.85	69.30	3427.43	4.92
-245	3419	65.52	70.02	3422.43	4.97
-250	3414	66.18	70.73	3417.43	5.01
-255	3409	66.84	71.43	3412.43	5.06
-260	3404	67.49	72.13	3407.43	5.10
-265	3399	68.13	72.83	3402.43	5.15
-270	3394	68.77	73.51	3397.43	5.19
-275	3389	69.40	74.19	3392.43	5.23
-280	3384	70.02	74.87	3387.43	5.28
-285	3379	70.65	75.53	3382.43	5.32
-290	3374	71.26	76.19	3377.43	5.36
-295	3369	71.87	76.85	3372.43	5.41
-300	3364	72.47	77.50	3367.43	5.45
-305	3359	73.07	78.15	3362.43	5.49
-310	3354	73.67	78.79	3357.43	5.53
-315	3349	74.26	79.42	3352.43	5.57
-320	3344	74.84	80.05	3347.43	5.61
-325	3339	75.43	80.67	3342.43	5.66
-330	3334	76.00	81.29	3337.43	5.70
-335	3329	76.57	81.91	3332.43	5.74
-340	3324	77.14	82.52	3327.43	5.78
-345	3319	77.70	83.13	3322.43	5.82
-350	3314	78.26	83.73	3317.43	5.86
-355	3309	78.82	84.33	3312.43	5.90
-360	3304	79.37	84.92	3307.43	5.94

Drop z ft	El. Lower nappe ft	Lower nappe distance from d/s parapet ft	Upper nappe distance from d/s parapet ft	El. Upper nappe ft	Jet width Bj ft
-365	3299	79.92	85.51	3302.43	5.97
-370	3294	80.46	86.09	3297.43	6.01
-375	3289	81.00	86.68	3292.43	6.05
-380	3284	81.54	87.25	3287.43	6.09
-385	3279	82.07	87.83	3282.43	6.13
-390	3274	82.60	88.40	3277.43	6.17
-395	3269	83.13	88.96	3272.43	6.20
-400	3264	83.65	89.53	3267.43	6.24
-405	3259	84.17	90.08	3262.43	6.28
-410	3254	84.69	90.64	3257.43	6.32
-415	3249	85.20	91.19	3252.43	6.35
-420	3244	85.71	91.74	3247.43	6.39
-425	3239	86.22	92.29	3242.43	6.43
-430	3234	86.72	92.83	3237.43	6.46
-435	3229	87.22	93.37	3232.43	6.50
-440	3224	87.72	93.91	3227.43	6.53
-445	3219	88.22	94.44	3222.43	6.57
-450	3214	88.71	94.97	3217.43	6.61
-455	3209	89.20	95.50	3212.43	6.64
-460	3204	89.69	96.02	3207.43	6.68
-465	3199	90.17	96.54	3202.43	6.71
-470	3194	90.66	97.06	3197.43	6.75
-475	3189	91.14	97.58	3192.43	6.78
-480	3184	91.61	98.09	3187.43	6.82
-485	3179	92.09	98.60	3182.43	6.85
-490	3174	92.56	99.11	3177.43	6.88
-495	3169	93.03	99.62	3172.43	6.92
-500	3164	93.50	100.12	3167.43	6.95
-505	3159	93.96	100.62	3162.43	6.99
-510	3154	94.43	101.12	3157.43	7.02
-515	3149	94.89	101.61	3152.43	7.05
-520	3144	95.34	102.11	3147.43	7.09
-525	3139	95.80	102.60	3142.43	7.12
-530	3134	96.25	103.09	3137.43	7.15
-535	3129	96.71	103.57	3132.43	7.19
-540	3124	97.16	104.06	3127.43	7.22
-545	3119	97.60	104.54	3122.43	7.25
-550	3114	98.05	105.02	3117.43	7.28

Table A4. - Trajectory locations for a reservoir head of 4 ft horizontal and drop (z) distances and elevations from the downstream parapet location. The trajectories include the spread of the jet due to gravity and turbulence.

Drop z ft	El. Lower nappe ft	Lower nappe distance from d/s parapet ft	Upper nappe distance from d/s parapet ft	El. Upper nappe ft	Jet width Bj ft
0	3664	0.00	0.00	3665.71	1.71
-1	3663	2.99	3.13	3664.71	1.31
-2	3662	4.25	4.41	3663.71	1.24
-3	3661	5.21	5.40	3662.71	1.18
-4	3660	6.01	6.23	3661.71	1.15
-5	3659	6.72	6.97	3660.71	1.12
-6	3658	7.36	7.63	3659.71	1.10
-7	3657	7.95	8.24	3658.71	1.08
-8	3656	8.50	8.81	3657.71	1.07
-9	3655	9.02	9.35	3656.71	1.06
-10	3654	9.50	9.86	3655.71	1.05
-14.64	3649.36	11.50	11.93	3651.07	1.04
-15	3649	11.64	12.08	3650.71	1.04
-20	3644	13.43	13.95	3645.71	1.05
-25	3639	15.01	15.60	3640.71	1.08
-29.27	3634.73	16.24	16.89	3636.44	1.10
-30	3634	16.44	17.10	3635.71	1.10
-35	3629	17.75	18.47	3630.71	1.13
-40	3624	18.98	19.75	3625.71	1.17
-45	3619	20.12	20.95	3620.71	1.20
-50	3614	21.21	22.08	3615.71	1.23
-55	3609	22.24	23.16	3610.71	1.26
-58.55	3605.45	22.95	23.90	3607.16	1.29
-60	3604	23.23	24.20	3605.71	1.30
-65	3599	24.17	25.19	3600.71	1.33
-70	3594	25.09	26.14	3595.71	1.36
-75	3589	25.96	27.06	3590.71	1.39
-80	3584	26.81	27.95	3585.71	1.42
-85	3579	27.64	28.81	3580.71	1.45
-87.82	3576.18	28.09	29.29	3577.89	1.47
-90	3574	28.44	29.65	3575.71	1.48
-95	3569	29.21	30.46	3570.71	1.51
-100	3564	29.97	31.26	3565.71	1.54
-105	3559	30.71	32.03	3560.71	1.57
-110	3554	31.43	32.79	3555.71	1.60
-115	3549	32.13	33.52	3550.71	1.63
-120	3544	32.82	34.25	3545.71	1.66
-125	3539	33.50	34.95	3540.71	1.69
-130	3534	34.16	35.65	3535.71	1.71
-131.73	3532.27	34.39	35.88	3533.98	1.72

Drop z ft	El. Lower nappe ft	Lower nappe distance from d/s parapet ft	Upper nappe distance from d/s parapet ft	El. Upper nappe ft	Jet width Bj ft
-135	3529	34.81	36.33	3530.71	1.74
-140	3524	35.45	37.00	3525.71	1.77
-145	3519	36.07	37.65	3520.71	1.79
-150	3514	36.69	38.30	3515.71	1.82
-155	3509	37.30	38.93	3510.71	1.84
-160	3504	37.89	39.56	3505.71	1.87
-165	3499	38.48	40.17	3500.71	1.89
-170	3494	39.06	40.78	3495.71	1.92
-175	3489	39.62	41.37	3490.71	1.94
-180	3484	40.19	41.96	3485.71	1.97
-185	3479	40.74	42.54	3480.71	1.99
-190	3474	41.28	43.11	3475.71	2.02
-195	3469	41.82	43.68	3470.71	2.04
-200	3464	42.36	44.23	3465.71	2.06
-205	3459	42.88	44.78	3460.71	2.08
-210	3454	43.40	45.33	3455.71	2.11
-215	3449	43.91	45.86	3450.71	2.13
-220	3444	44.42	46.40	3445.71	2.15
-225	3439	44.92	46.92	3440.71	2.17
-230	3434	45.42	47.44	3435.71	2.20
-235	3429	45.91	47.95	3430.71	2.22
-240	3424	46.39	48.46	3425.71	2.24
-245	3419	46.87	48.97	3420.71	2.26
-250	3414	47.35	49.46	3415.71	2.28
-255	3409	47.82	49.96	3410.71	2.30
-260	3404	48.28	50.44	3405.71	2.32
-265	3399	48.74	50.93	3400.71	2.34
-270	3394	49.20	51.41	3395.71	2.37
-275	3389	49.65	51.88	3390.71	2.39
-280	3384	50.10	52.35	3385.71	2.41
-285	3379	50.55	52.82	3380.71	2.43
-290	3374	50.99	53.28	3375.71	2.45
-295	3369	51.42	53.74	3370.71	2.47
-300	3364	51.86	54.19	3365.71	2.48
-305	3359	52.29	54.64	3360.71	2.50
-310	3354	52.71	55.09	3355.71	2.52
-315	3349	53.14	55.53	3350.71	2.54
-320	3344	53.56	55.97	3345.71	2.56
-325	3339	53.97	56.41	3340.71	2.58
-330	3334	54.38	56.84	3335.71	2.60
-335	3329	54.79	57.27	3330.71	2.62
-340	3324	55.20	57.70	3325.71	2.64
-345	3319	55.60	58.12	3320.71	2.66
-350	3314	56.01	58.54	3315.71	2.67
-355	3309	56.40	58.96	3310.71	2.69

Drop z ft	El. Lower nappe ft	Lower nappe distance from d/s parapet ft	Upper nappe distance from d/s parapet ft	El. Upper nappe ft	Jet width Bj ft
-360	3304	56.80	59.37	3305.71	2.71
-365	3299	57.19	59.78	3300.71	2.73
-370	3294	57.58	60.19	3295.71	2.75
-375	3289	57.97	60.60	3290.71	2.76
-380	3284	58.35	61.00	3285.71	2.78
-385	3279	58.74	61.40	3280.71	2.80
-390	3274	59.12	61.80	3275.71	2.82
-395	3269	59.49	62.19	3270.71	2.83
-400	3264	59.87	62.59	3265.71	2.85
-405	3259	60.24	62.98	3260.71	2.87
-410	3254	60.61	63.37	3255.71	2.88
-415	3249	60.98	63.75	3250.71	2.90
-420	3244	61.34	64.13	3245.71	2.92
-425	3239	61.71	64.52	3240.71	2.94
-430	3234	62.07	64.89	3235.71	2.95
-435	3229	62.43	65.27	3230.71	2.97
-440	3224	62.79	65.65	3225.71	2.99
-445	3219	63.14	66.02	3220.71	3.00
-450	3214	63.49	66.39	3215.71	3.02
-455	3209	63.85	66.76	3210.71	3.03
-460	3204	64.19	67.12	3205.71	3.05
-465	3199	64.54	67.49	3200.71	3.07
-470	3194	64.89	67.85	3195.71	3.08
-475	3189	65.23	68.21	3190.71	3.10
-480	3184	65.57	68.57	3185.71	3.11
-485	3179	65.91	68.93	3180.71	3.13
-490	3174	66.25	69.28	3175.71	3.15
-495	3169	66.59	69.63	3170.71	3.16
-500	3164	66.92	69.98	3165.71	3.18
-505	3159	67.26	70.33	3160.71	3.19
-510	3154	67.59	70.68	3155.71	3.21
-515	3149	67.92	71.03	3150.71	3.22
-520	3144	68.25	71.37	3145.71	3.24
-525	3139	68.57	71.71	3140.71	3.25
-530	3134	68.90	72.06	3135.71	3.27
-535	3129	69.22	72.40	3130.71	3.28
-540	3124	69.55	72.73	3125.71	3.30
-545	3119	69.87	73.07	3120.71	3.31
-550	3114	70.19	73.40	3115.71	3.33

Table A5. - Trajectory locations for a reservoir head of 2 ft horizontal and drop (z) distances and elevations from the downstream parapet location. The trajectories include the spread of the jet due

to gravity and turbulence.

Drop z ft	El. Lower nappe ft	Lower nappe distance from d/s parapet ft	Upper nappe distance from d/s parapet ft	El. Upper nappe ft	Jet width Bj ft
0	3664	0.00	0.00	3664.86	0.86
-1	3663	2.14	2.19	3663.86	0.59
-2	3662	3.03	3.10	3662.86	0.53
-3	3661	3.71	3.79	3661.86	0.50
-4	3660	4.28	4.38	3660.86	0.48
-5	3659	4.78	4.90	3659.86	0.46
-6	3658	5.24	5.36	3658.86	0.45
-7	3657	5.66	5.80	3657.86	0.44
-8	3656	6.05	6.20	3656.86	0.44
-9	3655	6.42	6.57	3655.86	0.44
-10	3654	6.76	6.93	3654.86	0.43
-14.64	3649.36	8.18	8.39	3650.22	0.43
-15	3649	8.28	8.49	3649.86	0.43
-20	3644	9.56	9.80	3644.86	0.44
-25	3639	10.68	10.96	3639.86	0.46
-29.27	3634.73	11.56	11.86	3635.59	0.47
-30	3634	11.70	12.01	3634.86	0.47
-35	3629	12.64	12.98	3629.86	0.49
-40	3624	13.51	13.87	3624.86	0.51
-45	3619	14.33	14.72	3619.86	0.52
-50	3614	15.10	15.51	3614.86	0.54
-55	3609	15.84	16.27	3609.86	0.56
-58.55	3605.45	16.34	16.79	3606.31	0.57
-60	3604	16.54	17.00	3604.86	0.57
-65	3599	17.21	17.69	3599.86	0.59
-70	3594	17.86	18.36	3594.86	0.60
-75	3589	18.49	19.00	3589.86	0.62
-80	3584	19.10	19.63	3584.86	0.63
-85	3579	19.68	20.23	3579.86	0.65
-87.82	3576.18	20.01	20.57	3577.04	0.66
-90	3574	20.25	20.82	3574.86	0.66
-95	3569	20.81	21.39	3569.86	0.68
-100	3564	21.35	21.95	3564.86	0.69
-105	3559	21.87	22.49	3559.86	0.71
-110	3554	22.39	23.02	3554.86	0.72
-115	3549	22.89	23.54	3549.86	0.73
-120	3544	23.38	24.04	3544.86	0.75
-125	3539	23.86	24.54	3539.86	0.76
-130	3534	24.34	25.03	3534.86	0.77
131.73	3532.27	24.50	25.19	3533.13	0.78
-135	3529	24.80	25.50	3529.86	0.78
-140	3524	25.25	25.97	3524.86	0.80
-145	3519	25.70	26.43	3519.86	0.81

Drop z ft	El. Lower nappe ft	Lower nappe distance from d/s parapet ft	Upper nappe distance from d/s parapet ft	El. Upper nappe ft	Jet width Bj ft
-150	3514	26.14	26.89	3514.86	0.82
-155	3509	26.57	27.33	3509.86	0.83
-160	3504	27.00	27.77	3504.86	0.85
-165	3499	27.41	28.20	3499.86	0.86
-170	3494	27.83	28.62	3494.86	0.87
-175	3489	28.23	29.04	3489.86	0.88
-180	3484	28.63	29.45	3484.86	0.89
-185	3479	29.03	29.86	3479.86	0.90
-190	3474	29.42	30.26	3474.86	0.91
-195	3469	29.80	30.66	3469.86	0.92
-200	3464	30.18	31.05	3464.86	0.94
-205	3459	30.55	31.43	3459.86	0.95
-210	3454	30.92	31.82	3454.86	0.96
-215	3449	31.29	32.19	3449.86	0.97
-220	3444	31.65	32.57	3444.86	0.98
-225	3439	32.01	32.93	3439.86	0.99
-230	3434	32.36	33.30	3434.86	1.00
-235	3429	32.71	33.66	3429.86	1.01
-240	3424	33.06	34.01	3424.86	1.02
-245	3419	33.40	34.37	3419.86	1.03
-250	3414	33.74	34.72	3414.86	1.04
-255	3409	34.07	35.06	3409.86	1.05
-260	3404	34.41	35.40	3404.86	1.06
-265	3399	34.73	35.74	3399.86	1.07
-270	3394	35.06	36.08	3394.86	1.08
-275	3389	35.38	36.41	3389.86	1.08
-280	3384	35.70	36.74	3384.86	1.09
-285	3379	36.02	37.07	3379.86	1.10
-290	3374	36.33	37.39	3374.86	1.11
-295	3369	36.65	37.71	3369.86	1.12
-300	3364	36.96	38.03	3364.86	1.13
-305	3359	37.26	38.35	3359.86	1.14
-310	3354	37.57	38.66	3354.86	1.15
-315	3349	37.87	38.97	3349.86	1.16
-320	3344	38.17	39.28	3344.86	1.17
-325	3339	38.46	39.59	3339.86	1.17
-330	3334	38.76	39.89	3334.86	1.18
-335	3329	39.05	40.19	3329.86	1.19
-340	3324	39.34	40.49	3324.86	1.20
-345	3319	39.63	40.79	3319.86	1.21
-350	3314	39.91	41.08	3314.86	1.22
-355	3309	40.20	41.37	3309.86	1.23
-360	3304	40.48	41.66	3304.86	1.23
-365	3299	40.76	41.95	3299.86	1.24
-370	3294	41.04	42.24	3294.86	1.25

Drop z ft	El. Lower nappe ft	Lower nappe distance from d/s parapet ft	Upper nappe distance from d/s parapet ft	El. Upper nappe ft	Jet width Bj ft
-375	3289	41.31	42.52	3289.86	1.26
-380	3284	41.59	42.81	3284.86	1.27
-385	3279	41.86	43.09	3279.86	1.27
-390	3274	42.13	43.37	3274.86	1.28
-395	3269	42.40	43.64	3269.86	1.29
-400	3264	42.67	43.92	3264.86	1.30
-405	3259	42.93	44.19	3259.86	1.31
-410	3254	43.20	44.47	3254.86	1.31
-415	3249	43.46	44.74	3249.86	1.32
-420	3244	43.72	45.01	3244.86	1.33
-425	3239	43.98	45.27	3239.86	1.34
-430	3234	44.24	45.54	3234.86	1.34
-435	3229	44.49	45.80	3229.86	1.35
-440	3224	44.75	46.07	3224.86	1.36
-445	3219	45.00	46.33	3219.86	1.37
-450	3214	45.25	46.59	3214.86	1.37
-455	3209	45.51	46.84	3209.86	1.38
-460	3204	45.75	47.10	3204.86	1.39
-465	3199	46.00	47.36	3199.86	1.40
-470	3194	46.25	47.61	3194.86	1.40
-475	3189	46.49	47.86	3189.86	1.41
-480	3184	46.74	48.11	3184.86	1.42
-485	3179	46.98	48.36	3179.86	1.43
-490	3174	47.22	48.61	3174.86	1.43
-495	3169	47.46	48.86	3169.86	1.44
-500	3164	47.70	49.11	3164.86	1.45
-505	3159	47.94	49.35	3159.86	1.45
-510	3154	48.18	49.60	3154.86	1.46
-515	3149	48.41	49.84	3149.86	1.47
-520	3144	48.65	50.08	3144.86	1.48
-525	3139	48.88	50.32	3139.86	1.48
-530	3134	49.11	50.56	3134.86	1.49
-535	3129	49.34	50.80	3129.86	1.50
-540	3124	49.57	51.04	3124.86	1.50
-545	3119	49.80	51.27	3119.86	1.51
-550	3114	50.03	51.51	3114.86	1.52

Appendix B

Jet Trajectories for 18, 12, 8 4 and 2 ft of reservoir overtopping heads.

Table B1. - Stream power density in the flow and the width of the jet per unit area at various elevations below Yellowtail Dam for the overtopping heads being investigated. The area of the jet is from the outer jet thickness of a unit width of flow and is assumed constant after jet break up for each flow rate. Jet break up and associated maximum stream power density is shown as the last row for each overtopping head.

Lower nappe El.	H = 18 ft				H = 12 ft				H = 8 ft				H = 4 ft				H = 2 ft			
	Jet width (Bj)	Total SP	SP per unit area		Jet width (Bj)	Total SP	SP per unit area		Jet width (Bj)	Total SP	SP per unit area		Jet width (Bj)	Total SP	SP per unit area		Jet width (Bj)	Total SP	SP per unit area	
ft	ft	(ft-lb/s/ft)	(ft-lb/s-ft^2)	(kW/m^2)	ft	(ft-lb/s/ft)	(ft-lb/s-ft^2)	(kW/m^2)	ft	(ft-lb/s/ft)	(ft-lb/s-ft^2)	(kW/m^2)	ft	(ft-lb/s/ft)	(ft-lb/s-ft^2)	(kW/m^2)	ft	(ft-lb/s/ft)	(ft-lb/s-ft^2)	(kW/m^2)
3664	7.71	225590.91	29267.87	427	5.14	81864.09	15931.41	232	3.43	29707.45	8671.96	127	1.71	5251.58	3066.00	45	0.86	928.36	1079.49	16
3663	7.02	238123.74	33901.58	495	4.46	88686.10	19883.72	290	2.84	33420.88	11768.91	172	1.31	6564.48	5023.50	73	0.59	1392.54	2368.35	35
3662	6.97	250656.57	35960.49	525	4.39	95508.11	21745.38	317	2.76	37134.31	13430.80	196	1.24	7877.38	6375.91	93	0.53	1856.72	3478.18	51
3661	6.92	263189.40	38006.04	555	4.34	102330.12	23602.66	344	2.71	40847.74	15100.02	220	1.18	9190.27	7758.76	113	0.50	2320.89	4638.62	68
3660	6.89	275722.23	40036.69	584	4.29	109152.12	25452.14	371	2.66	44561.17	16770.17	245	1.15	10503.17	9157.51	134	0.48	2785.07	5824.16	85
3659	6.85	288255.05	42051.20	614	4.25	115974.13	27291.04	398	2.62	48274.60	18436.19	269	1.12	11816.06	10561.65	154	0.46	3249.25	7018.30	102
3658	6.83	300787.88	44048.57	643	4.22	122796.14	29117.13	425	2.59	51988.03	20094.11	293	1.10	13128.96	11963.53	175	0.45	3713.43	8210.13	120
3657	6.81	313320.71	46027.99	672	4.19	129618.15	30928.62	451	2.56	55701.46	21740.83	317	1.08	14441.86	13357.56	195	0.44	4177.61	9392.38	137
3656	6.79	325853.54	47988.81	700	4.17	136440.15	32724.06	478	2.54	59414.89	23373.93	341	1.07	15754.75	14739.63	215	0.44	4641.79	10560.23	154
3655	6.78	338386.37	49930.54	729	4.15	143262.16	34502.34	504	2.53	63128.32	24991.53	365	1.06	17067.65	16106.80	235	0.44	5105.97	11710.50	171
3654	6.77	350919.20	51852.81	757	4.14	150084.17	36262.59	529	2.51	66841.75	26592.22	388	1.05	18380.54	17456.96	255	0.43	5570.15	12841.20	187
3649.36	6.77	409071.52	60445.57	882	4.11	181738.29	44179.42	645	2.49	84072.07	33774.08	493	1.04	24472.38	23467.71	342	0.43	7723.94	17809.93	260
3649	6.76	413583.34	61166.13	893	4.11	184194.21	44775.94	653	2.49	85408.91	34313.64	501	1.04	24945.02	23915.77	349				
3644	6.81	476247.48	69984.26	1021	4.13	218304.25	52796.90	771	2.50	103976.06	41542.13	606	1.05	31509.50	29869.35	436				
3639	6.88	538911.62	78328.47	1143	4.18	252414.29	60341.78	881	2.54	122543.21	48294.38	705	1.08	38073.98	35352.68	516				
3634.73	6.88	592426.80	86106.67	1257	4.24	281544.26	66434.43	970	2.58	138399.56	53714.28	784	1.10	43680.05	39706.12	579				
3634	6.98	601575.77	86231.48	1258	4.25	286524.32	67445.64	984	2.58	141110.37	54611.14	797								
3629	7.09	664239.91	93729.40	1368	4.32	320634.36	74148.72	1082	2.64	159677.52	60538.18	883								
3624	7.21	726904.05	100857.85	1472	4.41	354744.40	80490.55	1175	2.70	178244.67	66119.14	965								
3619	7.33	789568.19	107650.23	1571	4.50	388854.44	86507.63	1262	2.76	196811.82	71393.19	1042								
3614	7.47	852232.34	114137.06	1666	4.59	422964.48	92232.75	1346	2.82	215378.98	76394.63	1115								
3609	7.60	914896.48	120345.79	1756	4.68	457074.52	97694.88	1426	2.88	233946.13	81153.10	1184								
3605.45	6.77	959388.02	141761.89	2069	4.75	481292.65	101427.44	1480	2.93	247128.81	84398.28	1232								
3604	7.74	977560.62	126301.00	1843	4.77	491184.56	102919.49	1502												
3599	7.88	1040224.76	132024.57	1927	4.87	525294.60	107928.91	1575												
3594	8.02	1102888.91	137535.96	2007	4.96	559404.63	112742.74	1645												
3589	8.16	1165553.05	142852.49	2085	5.06	593514.67	117378.16	1713												
3584	8.30	1228217.19	147989.61	2160	5.15	627624.71	121850.31	1778												
3579	8.44	1290881.33	152961.08	2232	5.24	661734.75	126172.57	1841												
3576.18	6.77	1326223.91	195966.60	2860	5.30	680972.81	128548.73	1876												
3574	8.58	1353545.47	157779.23	2303																
3569	8.72	1416209.62	162455.12	2371																
3564	8.86	1478873.76	166998.69	2437																
3559	8.99	1541537.90	171418.89	2502																
3554	9.13	1604202.04	175723.82	2564																
3549	9.26	1666866.19	179920.81	2626																
3544	9.40	1729530.33	184016.53	2685																
3539	9.53	1792194.47	188017.04	2744																
3534	9.66	1854858.61	191927.88	2801																
3532.27	9.71	1876540.41	193261.09	2820																